DIFFRACTION IMAGE OF A FINITE SIZE OBJECT IN AN ANNULAR APERTURE SYSTEM

S. Sesnic, J. Fujita[+] and F. Pohl

IPP III/10 July 1973

MAX-PLANCK-INSTITUT FÜR PLASMAPHYSIK

GARCHING BEI MÜNCHEN

MAX-PLANCK-INSTITUT FÜR PLASMAPHYSIK

GARCHING BEI MÜNCHEN

DIFFRACTION IMAGE OF A FINITE SIZE OBJECT IN AN ANNULAR APERTURE SYSTEM

S. Sesnic, J. Fujita[+] and F. Pohl

IPP III/10 July 1973

[+]now at Institute of Plasma Physics,
Nagoya University, Nagoya 464, Japan

Die nachstehende Arbeit wurde im Rahmen des Vertrages zwischen dem Max-Planck-Institut für Plasmaphysik und der Europäischen Atomgemeinschaft über die Zusammenarbeit auf dem Gebiete der Plasmaphysik durchgeführt.

IPP III/10

S. Sesnic
J. Fujita
F. Pohl

Diffraction Image of a Finite Size Object in an Annular Aperture System

(in English)

July 1973

Abstract

The intensity and phase distributions near the geometrical focus of an error-free pencil of monochromatic light bounded by an annular aperture are obtained. The numerical results for a single point scatterer (point source) and for a cylindrical, homogeneous collection of stationary scatterers are discussed. If the central obstruction is kept small, an increase in the size of the scattering volume results in an increase in the size of the central image, across which the intensity and the phase are fairly constant. For medium and large central obstructions the numerical results indicate a very small or no change in the central image size if the scattering volume is increased. This might cause rather severe alignment restrictions if one wanted to use extreme forward laser scattering combined with wave mixing to study tokamak-like plasmas.

Table of Contents

List of Figures: Page

I. Introduction

We are investigating the problem of three-dimensional diffraction of a point or finite size source in an error-free axially symmetric optical system containing a ring-shaped aperture. The intensity and phase information are equally stressed in these studies. These investigations were prompted by a proposal[1] to study tokamak or stellarator-like plasma by utilizing an extreme forward laser scattering method in which the scattered light is either homodyned or heterodyned and the IF signal is then spectrum-analyzed to extract the information on the plasma. A similar problem might occur in laser communication and the results of this paper can be pertinent there, too.

Lommel[2] (1885) and Struve[3] (1886) were first to find the intensity distribution in an aberration-free image of a point source in a circular, axially symmetric optical system. For this purpose Lommel introduced new kind of functions, which are called Lommel functions after him. Utilizing Lommel-Struve theory, Zernike and Nijboer[4] (1949) were first to publish the intensity distribution near the geometrical focus. Linfoot and Wolf[5] (1952) applied this theory to telescopic star images by studying only the intensity distribution and the circular aperture. Later (1952) they obtained numerical results of the intensity distribution for an annular aperture[6] - the problem that was earlier investigated by Steward[7] (1925). In a more recent paper Linfoot and Wolf[8] (1956) evaluated the phase distribution near the focus in an aberration-free diffraction image. This was done for a circular aperture and a point source only.

We are extending these results in the case of an annular aperture by expressing the solutions in terms of three instead of - as done earlier[6] - two regions in order to obtain better convergence of the solutions. We also study the phase distribution for the case of a point source and annular aperture, which was not investigated earlier.

Finally, on the basis of a particular model we study the influence of an increased source size on the intensity and phase distributions near the focus.

In Sec. II the problem is defined. In Sec. III A and B the theoretical preliminaries for the point source case are given and some special cases are discussed. Sec. III C is devoted to presentation of numerical results for the point source case. In Sec. IV A the model and the computation method for the finite source case are discussed. Sec. IV B presents the results of the numerical calculation of the finite source case. Finally, in Sec. V the results of these calculations are summarized and the conclusions from these investigations are drawn.

II. Statement of Problem

This work was motivated by Gondhalekar and Keilmann[1], who proposed an extreme forward scattering experiment to measure the ion temperature. The same method can be utilized to study the spectrum of the waves in the plasma. A very simplified diagram of their method is shown in Fig. 1. A pulsed CO_2-laser beam is scattered from the plasma and the scattered radiation is collected by a lens and beam obstruction configuration such that the scattering angle is of the order of 10 mrad and the hollow collection cone has about 2 mrad. This scattered radiation is then focused on a mixer. The false light coming through the optical system can be used as a local oscillator. The mixer is a very fast cryogenic detector capable of several ns response time. The mixing is done

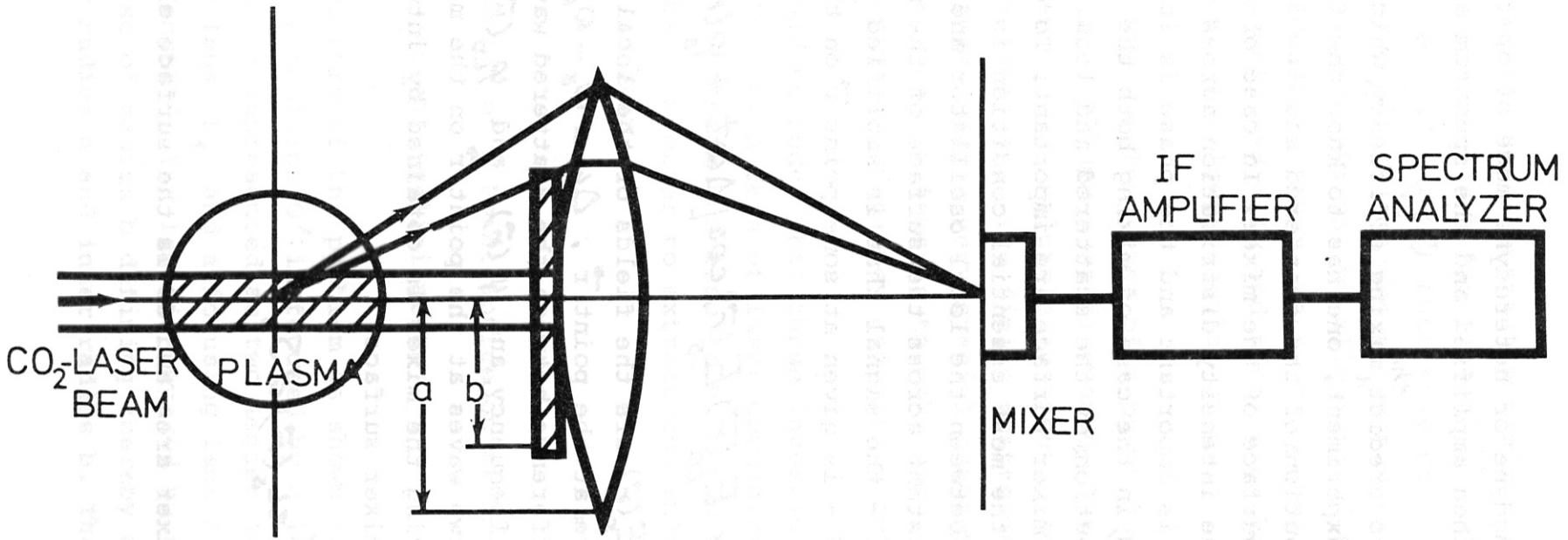

Fig. 1 Schematic diagram of the optical set-up for the extreme forward scattering experiment

in either the homodyne or heterodyne mode of operation. The mixed signal is then amplified and the spectrum analyzed.

To be able to predict the mixing efficiency, which is important in this experiment, one has to know the intensity and phase distributions of the scattered and the local oscillator waves across the surface of the mixer. In case of ordinary detection, only the intensity distribution across the detector surface is important and the phase is irrelevant. On the other hand, in the case of mixing both the intensity and phase distributions of the scattered and local oscillator waves across the mixer surface are important. To obtain efficient mixing, the most essential condition is that the phase difference between the local oscillator and scattered waves be constant across the surface of the mixer. The difference signal - the signal that is amplified and spectrum-analyzed - is given at some point $\vec{r}$ on the mixer by

$$u_s(\vec{r}) \sim E_{LO}(\vec{r})\, E_s(\vec{r}) \cos\left[\Delta\omega t + \varphi_s(\vec{r}) - \varphi_{LO}(\vec{r})\right],$$

where $E_{LO}(\vec{r})$ and $E_s(\vec{r})$ are the fields of the local oscillator and scattered waves at the point $\vec{r}$, $\Delta\omega = \omega_s - \omega_{LO}$ is the frequency difference between the scattered wave and the local oscillator frequency, and $\varphi_s(\vec{r})$ and $\varphi_{LO}(\vec{r})$ are the phases of these two waves at the point $\vec{r}$ on the mixer. The total signal leaving the mixer is obtained by integrating $u_s(\vec{r})$ over the mixer surface

$$U_s = \int_A u_s(\vec{r})\, dS,$$

where A is the mixer area and dS is the surface element.

To obtain for some constant $\hat{t}$ a maximum signal U_s , u_s should not oscillate as a function of $\vec{r}$, which means that the difference $\varphi_s(\vec{r}) - \varphi_{LO}(\vec{r})$ must stay constant on the mixer surface. This condition on the phase necessitates very stringent requirements on the alignment of the scattered and local oscillator waves. These two waves have to be aligned very well radially and their axes have to coincide to within a small allowed angular error.

First, the simplest case of a point source - or a very small scattering volume - is discussed. The information thus obtained is very valuable in understanding the finite scattering volume case. The finite scattering volume case is investigated under a very special scattering condition that, nevertheless, allows us to make some conclusions regarding the mixing efficiency and mixing optimization.

It should be added that these investigations can be easily adapted for a case of laser communication, where the laser carrier beam has also to be mixed with a local oscillator beam in order to extract the information carried by the carrier beam.

III. Diffraction of a Point Source on an Annular Aperture

A) Theoretical Preliminaries

The geometry of the problem is shown in Fig. 2. A point source at the position O′ is focused by a lens into point O. The lens is represented as two lenses in series: a collimating lens L_1 and a focusing lens L of diameter 2a and focal length f. The lens is covered by a concentric circular disc of radius b defining thereby an annular aperture of an outer radius a and inner radius b. The ratio of these

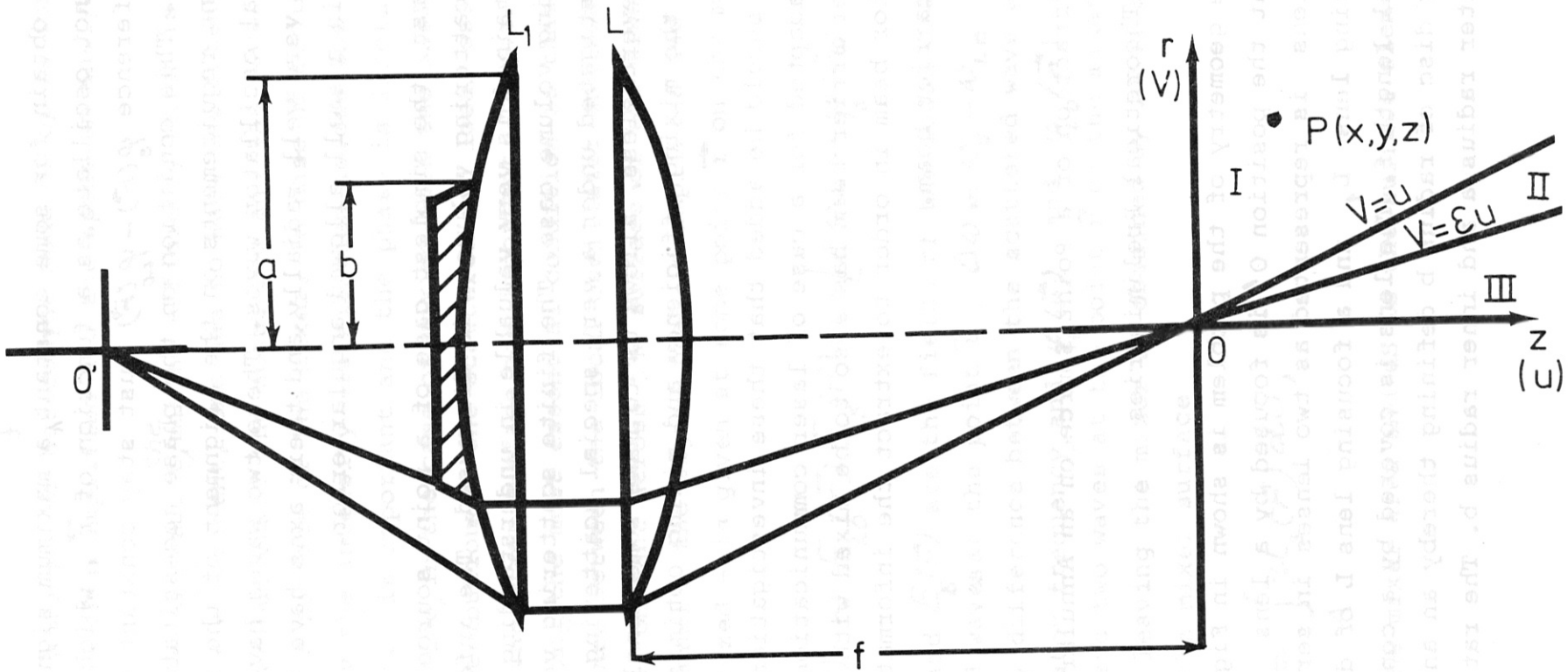

Fig. 2 Geometry of the diffraction problem

two radii defines the obstruction coefficient $\varepsilon = b/a$. Two conical sets of extreme rays passing the tips of the obstruction disc and the lens will separate the half-space near the focus into three regions: I, II and III as indicated in Fig. 2. I and III are the shadow regions and II is the illuminated region.

Using the Huygens-Fresnel principle, the complex displacement at the observation point P(x,y,z) near the focus can be written as

$$U(P) = -\frac{i}{\lambda}\frac{A}{f}\iint_W \frac{\exp[ik(s-f)]}{s}\,dS\,, \qquad (1)$$

where A/f is the amplitude of the wave in the annular aperture, dS is the surface element on the annular aperture, s is the distance between the surface element and the point P, and $k = 2\pi/\lambda$ is the wave number. If, additionally, $f \gg a \gg \lambda$ and the point P is very near to the focus, i.e. only few fringes away, the complex displacement becomes

$$U(P) = -\frac{i}{\lambda}\pi\left(\frac{a}{f}\right)^2 A \exp\left[i\left(\frac{f}{a}\right)^2 u\right]\left\{C(u,v) - iS(u,v)\right\}, \qquad (2)$$

where C(u,v) and S(u,v) are integrals which for a point source have the form:

$$C_P(u,v) = 2\int_\varepsilon^1 J_0(v\varrho)\cos\left(\tfrac{1}{2}u\varrho^2\right)\varrho\,d\varrho \qquad (3)$$

$$S_P(u,v) = 2\int_\varepsilon^1 J_0(v\varrho)\sin\left(\tfrac{1}{2}u\varrho^2\right)\varrho\,d\varrho \qquad (4)$$

and u and v are normalized coordinates defined as

$$u = \frac{2\pi}{\lambda}\left(\frac{a}{f}\right)^2 z \tag{5}$$

$$v = \frac{2\pi}{\lambda}\left(\frac{a}{f}\right) r, \tag{6}$$

$r^2 = x^2 + y^2$ and J_o is the Bessel function of the first kind.

The integrals (3) and (4) can be evaluated in terms of Lommel functions, which Lommel introduced for this purpose

$$U_n(u,v) = \sum_{m=0}^{\infty} (-1)^m \left(\frac{u}{v}\right)^{n+2m} J_{n+2m}(v) \tag{7}$$

and

$$V_n(u,v) = \sum_{m=0}^{\infty} (-1)^m \left(\frac{v}{u}\right)^{n+2m} J_{n+2m}(v), \tag{8}$$

where J_{n+2m} are again Bessel functions of the first kind.

These functions converge differently in each one of the three regions. In the region I, where $v > u$, U_n functions converge faster than V_n functions and conversely in the region III, where $\varepsilon u > v$, the functions V_n will converge faster. In the region II, on the other hand, a proper combination of U_n and V_n functions will converge in a fastest manner.

The expressions for the C_p and S_p for the three regions can be shown to have the following forms:

(a) Region I: $|u/v| \leq 1$

$$C_p(u,v) = \frac{\cos\frac{1}{2}u}{\frac{1}{2}u} U_1(u,v) + \frac{\sin\frac{1}{2}u}{\frac{1}{2}u} U_2(u,v) - \tag{9}$$

$$-\varepsilon^2\left\{\frac{\cos\frac{1}{2}u\varepsilon^2}{\frac{1}{2}u\varepsilon^2} U_1(u\varepsilon^2, v\varepsilon) + \frac{\sin\frac{1}{2}u\varepsilon^2}{\frac{1}{2}u\varepsilon^2} U_2(u\varepsilon^2, v\varepsilon)\right\}$$

$$S_p(u,v) = \frac{\sin\frac{1}{2}u}{\frac{1}{2}u} U_1(u,v) - \frac{\cos\frac{1}{2}u}{\frac{1}{2}u} U_2(u,v) - \tag{10}$$

$$-\varepsilon^2\left\{\frac{\sin\frac{1}{2}u\varepsilon^2}{\frac{1}{2}u\varepsilon^2} U_1(u\varepsilon^2, v\varepsilon) - \frac{\cos\frac{1}{2}u\varepsilon^2}{\frac{1}{2}u\varepsilon^2} U_2(u\varepsilon^2, v\varepsilon)\right\}.$$

(b) Region II: $1 \leq |u/v| \leq 1/\varepsilon$

$$C_p(u,v) = \frac{2}{u}\sin\frac{v^2}{2u} + \frac{\sin\frac{1}{2}u}{\frac{1}{2}u} V_0(u,v) - \frac{\cos\frac{1}{2}u}{\frac{1}{2}u} V_1(u,v) - \tag{11}$$

$$-\varepsilon^2\left\{\frac{\cos\frac{1}{2}u\varepsilon^2}{\frac{1}{2}u\varepsilon^2} U_1(u\varepsilon^2, v\varepsilon) + \frac{\sin\frac{1}{2}u\varepsilon^2}{\frac{1}{2}u\varepsilon^2} U_2(u\varepsilon^2, v\varepsilon)\right\}$$

$$S_p(u,v) = \frac{2}{u}\cos\frac{v^2}{2u} - \frac{\cos\frac{1}{2}u}{\frac{1}{2}u} V_0(u,v) - \frac{\sin\frac{1}{2}u}{\frac{1}{2}u} V_1(u,v) - \tag{12}$$

$$-\varepsilon^2\left\{\frac{\sin\frac{1}{2}u\varepsilon^2}{\frac{1}{2}u\varepsilon^2} U_1(u\varepsilon^2, v\varepsilon) - \frac{\cos\frac{1}{2}u\varepsilon^2}{\frac{1}{2}u\varepsilon^2} U_2(u\varepsilon^2, v\varepsilon)\right\}.$$

(c) Region III: $|u/v| \geq 1/\varepsilon$

$$C_p(u,v) = \frac{\sin\frac{1}{2}u}{\frac{1}{2}u} V_0(u,v) - \frac{\cos\frac{1}{2}u}{\frac{1}{2}u} - \tag{13}$$

$$-\varepsilon^2\left\{\frac{\sin\frac{1}{2}u\varepsilon^2}{\frac{1}{2}u\varepsilon^2} V_0(u\varepsilon^2, v\varepsilon) - \frac{\cos\frac{1}{2}u\varepsilon^2}{\frac{1}{2}u\varepsilon^2} V_1(u\varepsilon^2, v\varepsilon)\right\}$$

$$S_p(u,v) = -\frac{\cos\frac{1}{2}u}{\frac{1}{2}u} V_0(u,v) - \frac{\sin\frac{1}{2}u}{\frac{1}{2}u} + \tag{14}$$

$$+\varepsilon^2\left\{\frac{\cos\frac{1}{2}u\varepsilon^2}{\frac{1}{2}u\varepsilon^2} V_0(u\varepsilon^2, v\varepsilon) + \frac{\sin\frac{1}{2}u\varepsilon^2}{\frac{1}{2}u\varepsilon^2} V_1(u\varepsilon^2, v\varepsilon)\right\}.$$

Knowing the C and S functions for either a point or a finite size source, one can obtain the normalized intensity distribution and the phase distribution from

$$I(u,v) = \frac{1}{1-\varepsilon^2}\left(\frac{\lambda}{\pi}\right)^2\left(\frac{f}{a}\right)^4 \frac{1}{A^2} U(P)\cdot U^*(P) = \frac{1}{1-\varepsilon^2}\left[C^2(u,v) + S^2(u,v)\right] \tag{15}$$

and

$$\Phi(u,v) = \frac{\pi}{2} + \left(\frac{f}{a}\right)^2 u - \tan^{-1}\frac{S(u,v)}{C(u,v)} \,. \tag{16}$$

The intensity is normalized by assuming that the total power incident on the aperture is a constant of ε. This means that the power density is not constant but is proportional to $1/(1-\varepsilon^2)$. The intensity and phase distributions are axially symmetric around the optical axis and mirror symmetric around the focal plane u = 0.

B) Special Cases

It is of interest to observe the behavior of C and S functions in the focal plane and along the optical axis for various obstruction coefficients ε. The behavior of these special case functions will give us a clue about the effect of a finite source on the intensity and phase distributions.

(a) Distribution in the Focal Plane

In this case, u = 0 and one can show that the expressions (9) to (14) reduce to

$$C_p(0,v) = \frac{2}{v}\left[J_1(u) - \varepsilon J_1(\varepsilon v)\right] \qquad (17)$$

and

$$S_p(0,v) = 0.$$

A set of C_p functions for various ε is shown in Fig. 3. One can observe that by increasing the obstruction coefficient the first zero of the C_p function moves toward smaller v. The same can be concluded for higher order zeros, only the motion of the zero as ε increases oscillates slightly before it moves toward smaller v.

Indeed, one can show that by increasing ε from 0 to 1 the first zero moves from a certain maximum value of v to a certain minimum value. These values of v are just solutions of a transcendental equation

$$J_1(v) - \varepsilon J_1(\varepsilon v) = 0, \qquad (18)$$

where ε is a parameter.

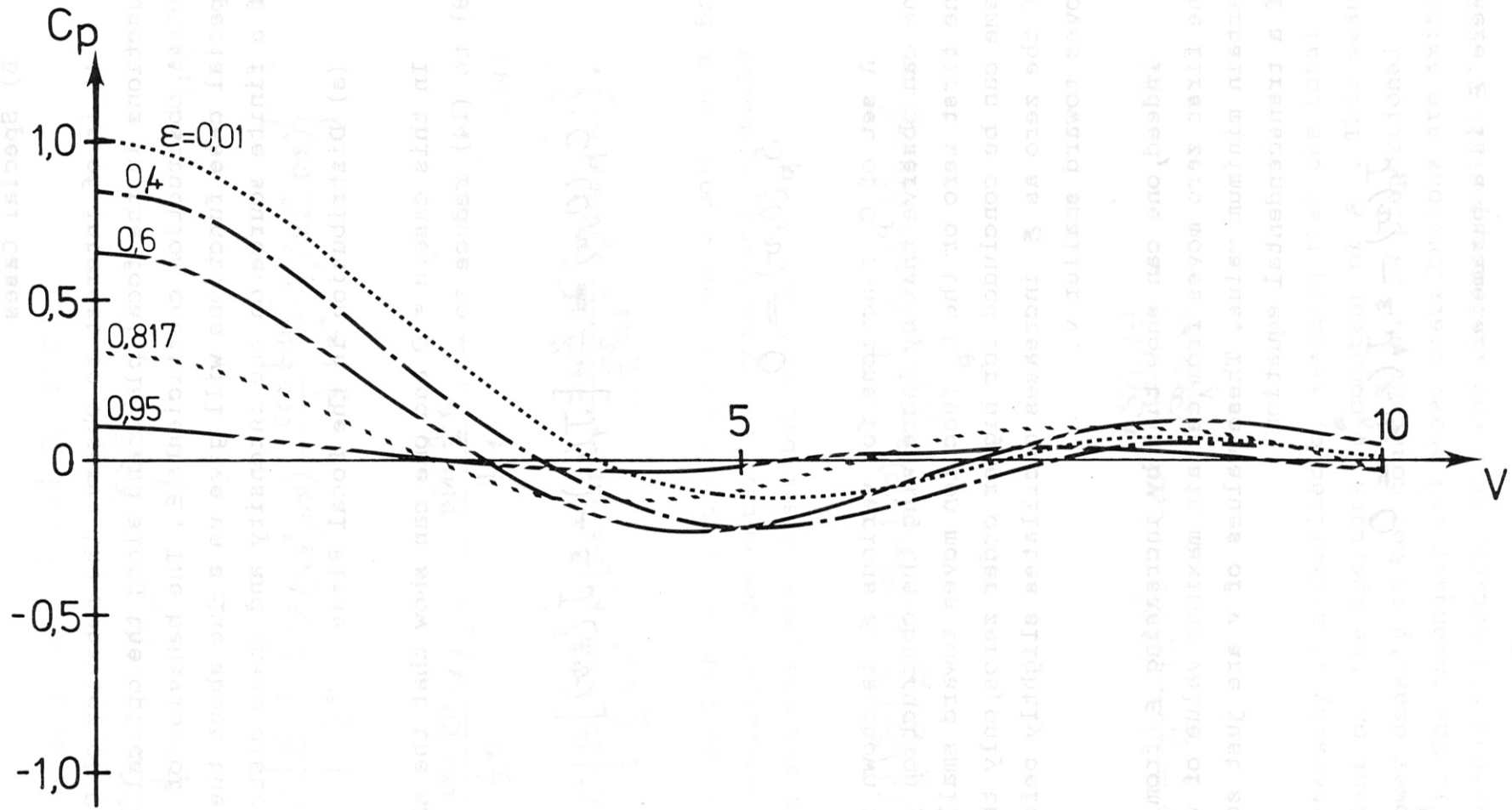

Fig. 3 Variation of the displacement function $C_p = C_p(0,v)$ in the focal plane for various obstruction coefficients ε.

For $\varepsilon = 0$ the first zero is just the root of the Bessel function $J_1(v) = 0$, i.e. $v_o = 3.83$. If ε is almost equal to 1, one can put $\varepsilon = 1 - \delta$, where $\delta \ll 1$ and then expand $J_1(\varepsilon v)$ in terms of the small parameter δ and higher order Bessel functions. The relation (18) will then reduce to $J_o(v) = 0$, which then means that the roots of (18) for the extreme case of $\varepsilon = 1$ (full blocking of the aperture) are just the roots of $J_o(v)$ function. The first root of the $J_o(v)$ is $v_o = 2.4$. Obviously, the first minima of the C_p function and, therefore, intensity lie for various obstruction coefficients ε between $v_o = 3.83$ and $v_o = 2.4$ values.

(b) Distribution along the Axis

Plugging $v = 0$ into expressions (9) to (14), one obtains

$$C_p(u,0) = \frac{4}{u} \sin\left[\frac{1}{4} u(1-\varepsilon^2)\right] \cos\left[\frac{1}{4}(1+\varepsilon^2)u\right] \qquad (19)$$

and

$$S_p(u,0) = \frac{4}{u} \sin\left[\frac{1}{4} u(1-\varepsilon^2)\right] \sin\left[\frac{1}{4} u(1+\varepsilon^2)\right]. \qquad (20)$$

Zeros of these functions are given by $u_1 = \frac{4m\pi}{1+\varepsilon^2}$ and $u_2 = \frac{4m\pi}{1-\varepsilon^2}$ for the Sp function and $u_1 = \frac{2(2m+1)\pi}{1+\varepsilon^2}$ and $u_2 = \frac{4m\pi}{1-\varepsilon^2}$ for the Cp function, where $m = 0, \pm 1, \pm 2 \ldots$. Increasing ε, the u_1-zeros move toward smaller u's and the u_2-zeros toward larger u's. This can be seen in Fig. 4, where these two

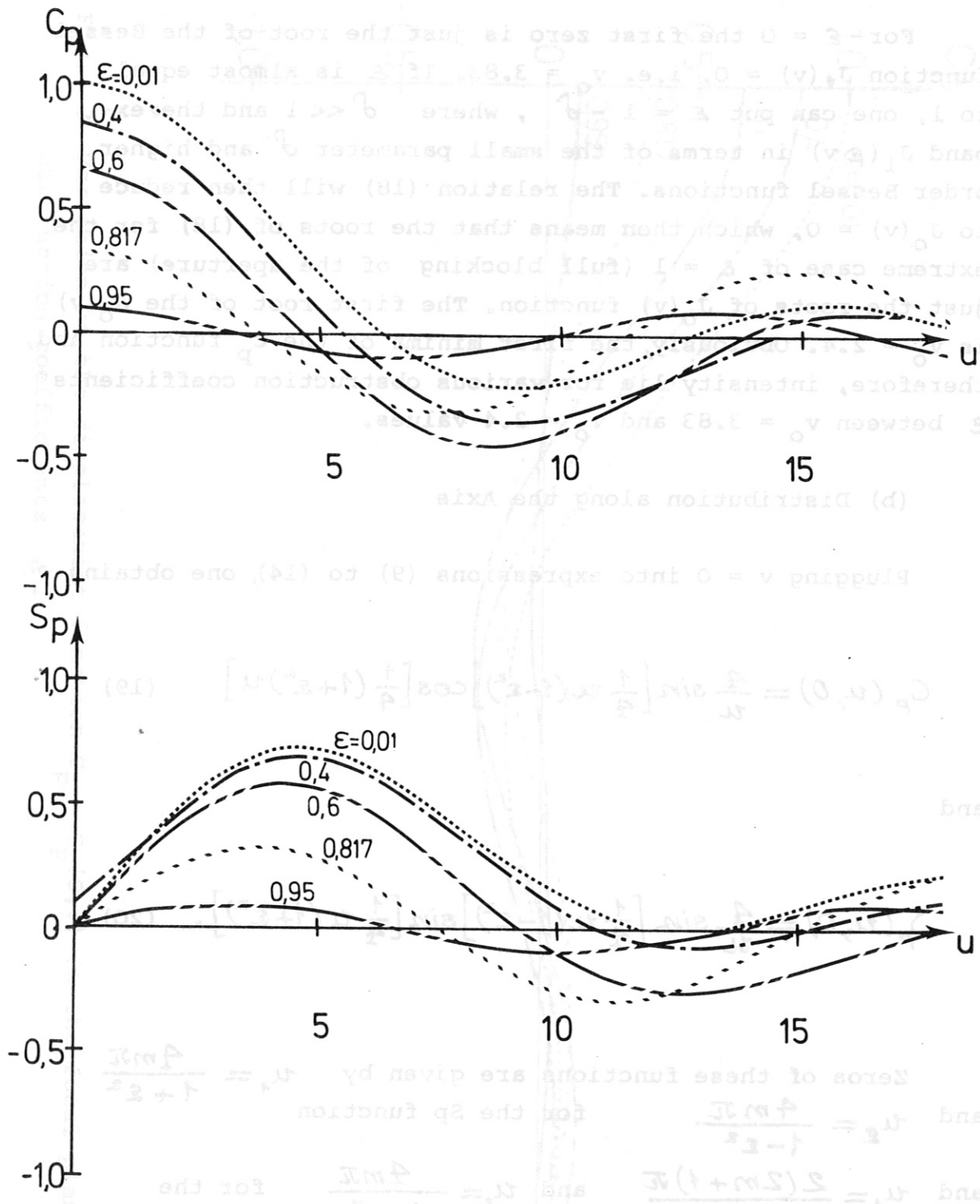

Fig. 4 Variation of displacement functions $C_p = C_p(u,o)$ and $S_p(u,0)$ along the optical axis for various obstruction coefficients ε.

functions are depicted with ε as a parameter. The intensity will fall to zero when a C_p-zero coincides with an S_p-zero. The normalized intensity distribution is given with a known[6] formula:

$$I(u,0) = (1-\varepsilon^2)^2 \left\{ \frac{\sin\left[\frac{1}{4}u(1-\varepsilon^2)\right]}{\frac{1}{4}u(1-\varepsilon^2)} \right\}^2 . \qquad (21)$$

It will be shown later that the isophotes (surfaces of constant intensity) are of ellipsoidal form very near the focus and of a general toroidal form for some distance away from the focus. The optical axis is the axis of symmetry for these surfaces. Increasing ε, these surfaces are slightly compressed in the radial direction but very strongly elongated in the axial direction. The elongation factor on the optical axis is found from (21) to be $1/(1-\varepsilon^2)$. From the earlier discussion it follows that the maximum compression ratio for the Airy disc is equal to 1.6, which is the ratio of the first root for $J_1(v)$ - corresponding to the $\varepsilon = 0$ case - and the first root of $J_0(v)$ - corresponding to the $\varepsilon \to 1$ case. The compression is therefore a very weak function of ε. The elongation is much more pronounced. It should be added that compression means better resolution and elongation represents an increase in optical depth.

C) Numerical Results for the Point Source

The intensity and phase distributions were numerically evaluated on a computer for various obstruction coefficients ε utilizing the relations (9) to (14) for C_p and S_p for the three regions and the relations (15) and (16) for the intensity and phase. The results of these calculations are shown in Figs. 5 to 12 . In the upper part of Fig. 5 the surfaces of constant intensity - the isophotes - are shown for an obstruction coefficient very close to zero. The surfaces of constant phase are shown beneath and in the vicinity of two characteristic planes normal to the optical axis. Very near the focal plane - u = 0 - these surfaces are plane and experience a sudden jump of π at the radial distances v at which the intensity becomes zero. Another characteristic plane is the plane at which the intensity in the focus decreases by 20 % on the optical axis. This position is important because it defines the length of the object that can be successfully imaged. For a very small ε it occurs around the plane $u_{20\%} = 3$. Note that the constant phase surfaces are much smoother now but still retain a faster phase change around the values of v at which the intensity goes to zero. This phase behavior is an important item of information for the mixing if the signal comes from an elongated object and the local oscillator is not specified. This point will be more thoroughly discussed in the section on the finite volume sources.

The effect of increasing ε is shown in subsequent figures. For obstruction ratios ε = 0.25, 0.6 and 0.95 the phase behavior is not shown, but for the cases ε = 0.4 and 0.817 it is again shown. The intensity distributions show indeed the trend that by increasing ε the isophotes are slightly compressed in the radial direction but are very much elongated in the axial direction. Note also that the complexity

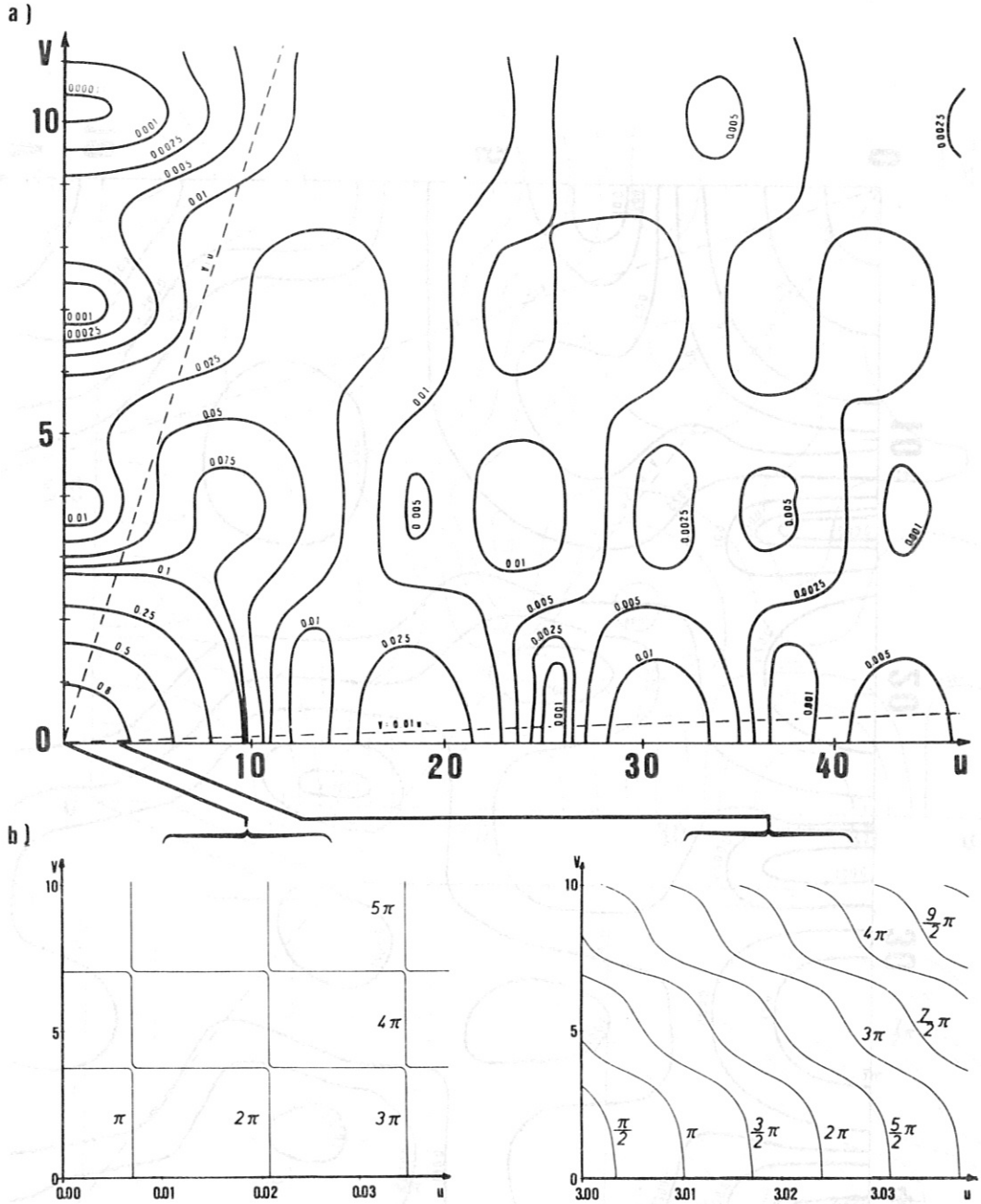

Fig. 5 Diffraction near the focus of an aberration-free pencil for an obstruction coefficient $\varepsilon = 0.01$. (a) Isophotes (lines of equal intensity) $I(u,v) = \text{Const}$ are shown. The dotted lines represent the boundaries of the hollow geometrical cone of rays. The diagram possesses axial symmetry around the u-axis and mirror symmetry around the focal plane u = 0. (b) Co-phasal surfaces $\Phi(u,v) = \text{Const}$ in the immediate neighborhood of the focal plane u = 0 and around u = 3.0 for f/a = 15. The jumps in phase occur in the Airy dark rings.

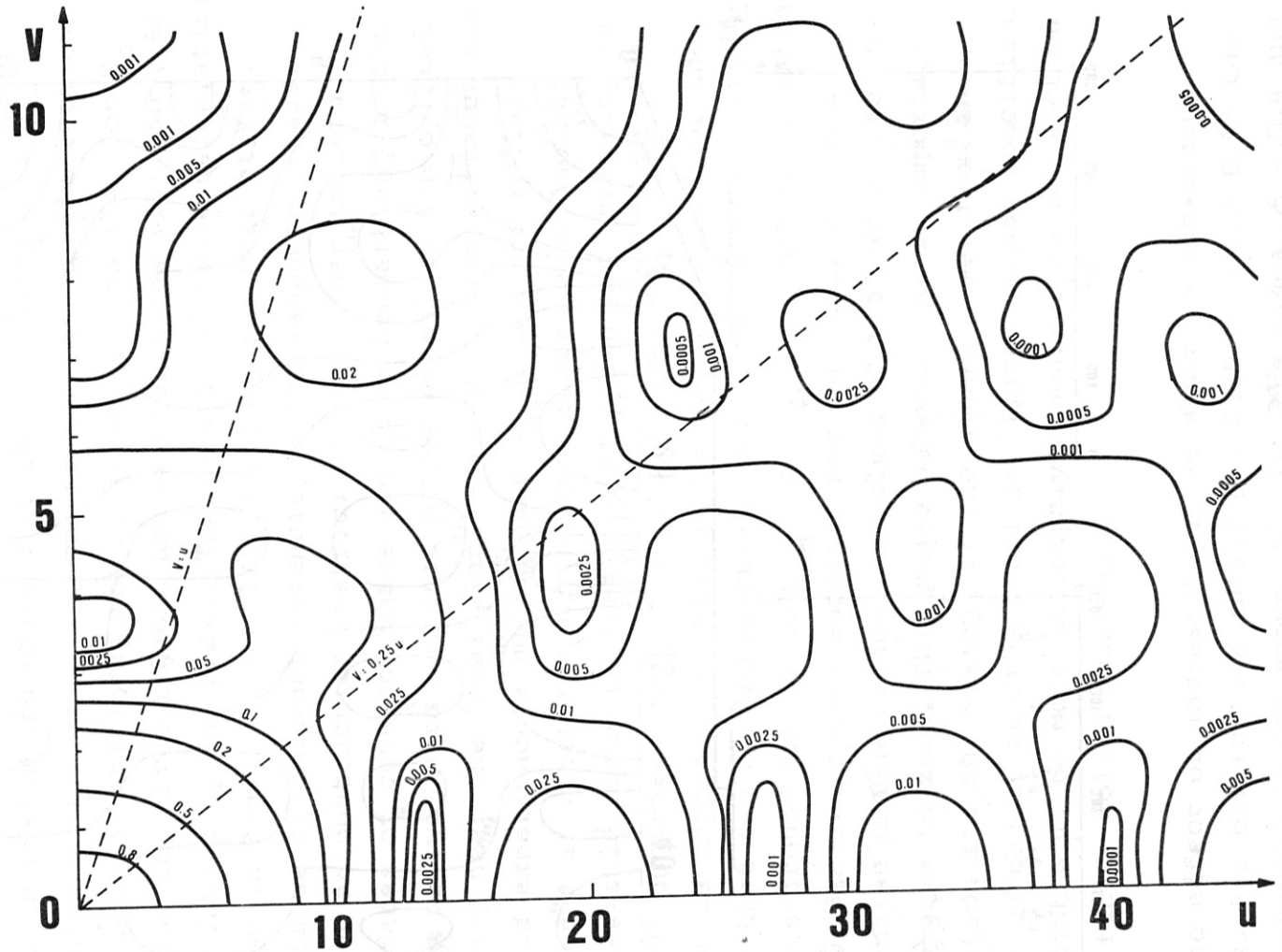

Fig. 6 Isophotes near the focus of an aberration-free pencil for an obstruction coefficient $\varepsilon = 0.25$.

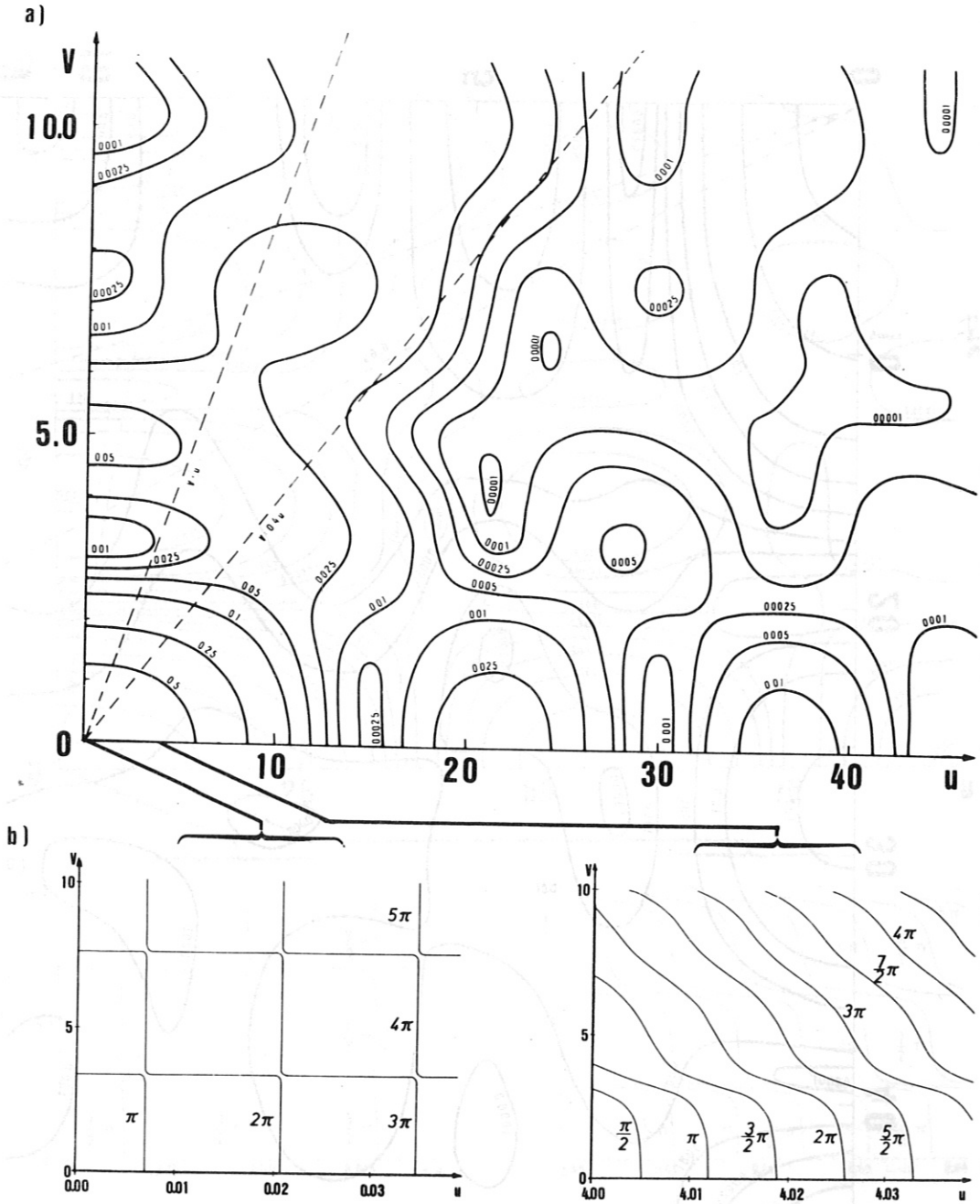

Fig. 7 Diffraction near the focus of an aberration-free pencil for an obstruction coefficient $\varepsilon = 0.4$. (a) Isophotes. (b) Co-phasal surfaces in the immediate neighborhood of the focal plane u = 0 and around u = 4.0 for f/a = 15.

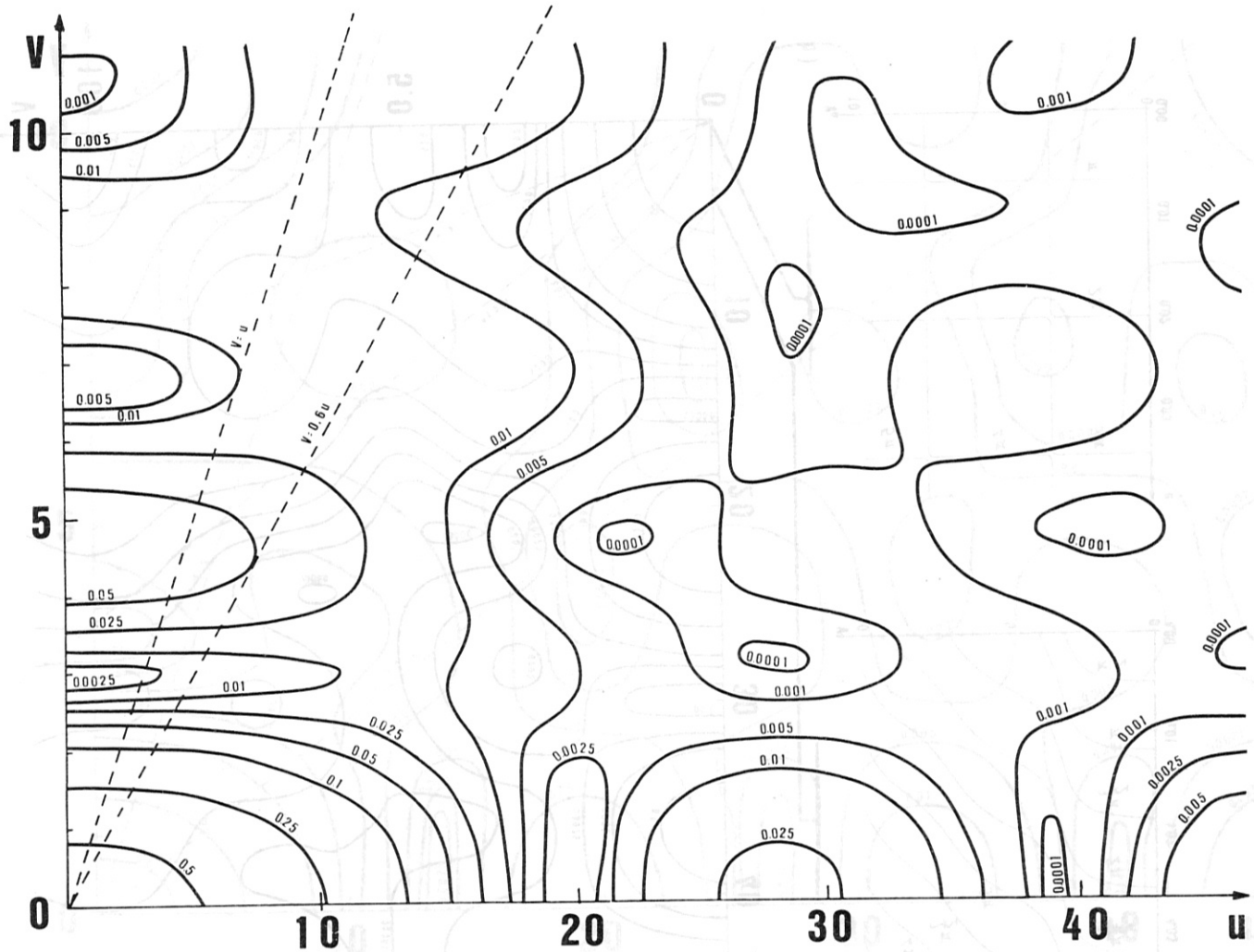

Fig. 8 Isophotes near the focus of an aberration-free pencil for an obstruction coefficient $\varepsilon = 0.6$.

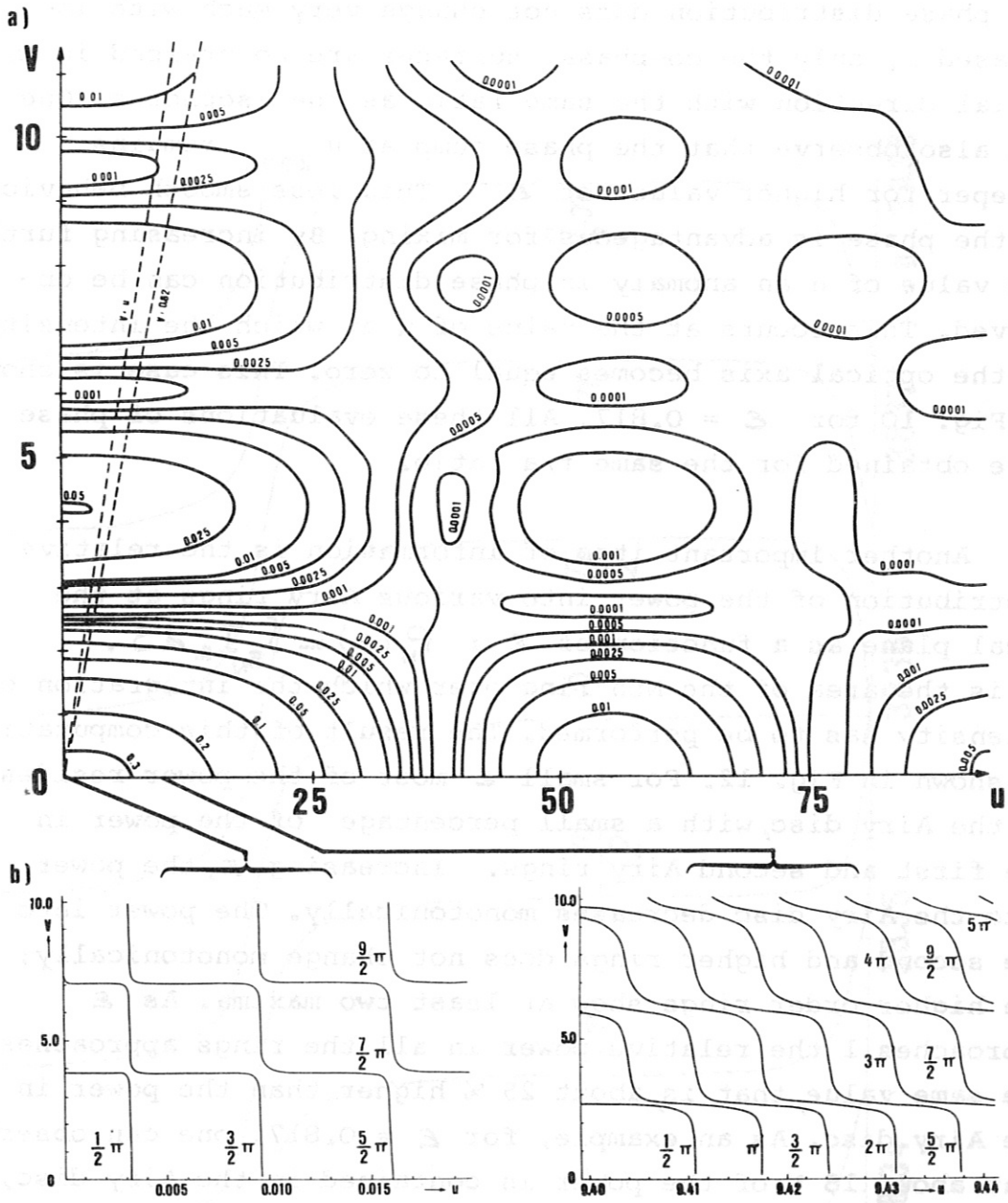

Fig. 9 Diffraction near the focus of an aberration-free pencil for an obstruction coefficient $\varepsilon = 0.817$ (a) Isophotes. (b) Cophasal surfaces in the immediate neighborhood of the focal plane u = 0 and around u = 9.4 for f/a = 15.

of the intensity distribution is decreased by increasing ε. The phase distribution does not change very much with increased ε, only the co-phasal surfaces are compressed in the radial direction with the same ratio as the isophotes. One can also observe that the phase jump at $u_{20\%}$ remains steeper for higher values of ε. This less smooth behavior of the phase is advantageous for mixing. By increasing further the value of u an anomaly in phase distribution can be observed. This occurs at the value of u at which the intensity on the optical axis becomes equal to zero. This case is shown in Fig. 10 for $\varepsilon = 0.817$. All these evaluations of phase were obtained for the same f/a ratio.

Another important item of information is the relative distribution of the power into various Airy rings at the focal plane as a function of ε : $P_N(\varepsilon) = \int_{S_N} I_\varepsilon \, dS$. S_N is the area of the Nth ring over which the integration of the intensity has to be performed. The result of this computation is shown in Fig. 12. For small ε most of the power resides in the Airy disc, with a small percentage of the power in the first and second Airy rings. Increasing ε, the power into the Airy disc decreases monotonically. The power into the second and higher rings does not change monotonically: the higher order rings show at least two maxima. As ε approaches 1 the relative power in all the rings approaches the same value, that is, about 25 % higher than the power in the Airy disc. As an example, for $\varepsilon = 0.817$, one can observe that about 18 % of the power is contained in the Airy disc, 22 % in the first, 20 % in the second, 17 % in the third, 13 % in the fourth, 9 % in the fifth, etc. ring. It follows that an increase in ε is detrimental to power collecting efficiency if the power is collected by a detector or mixer that covers only the Airy disc.

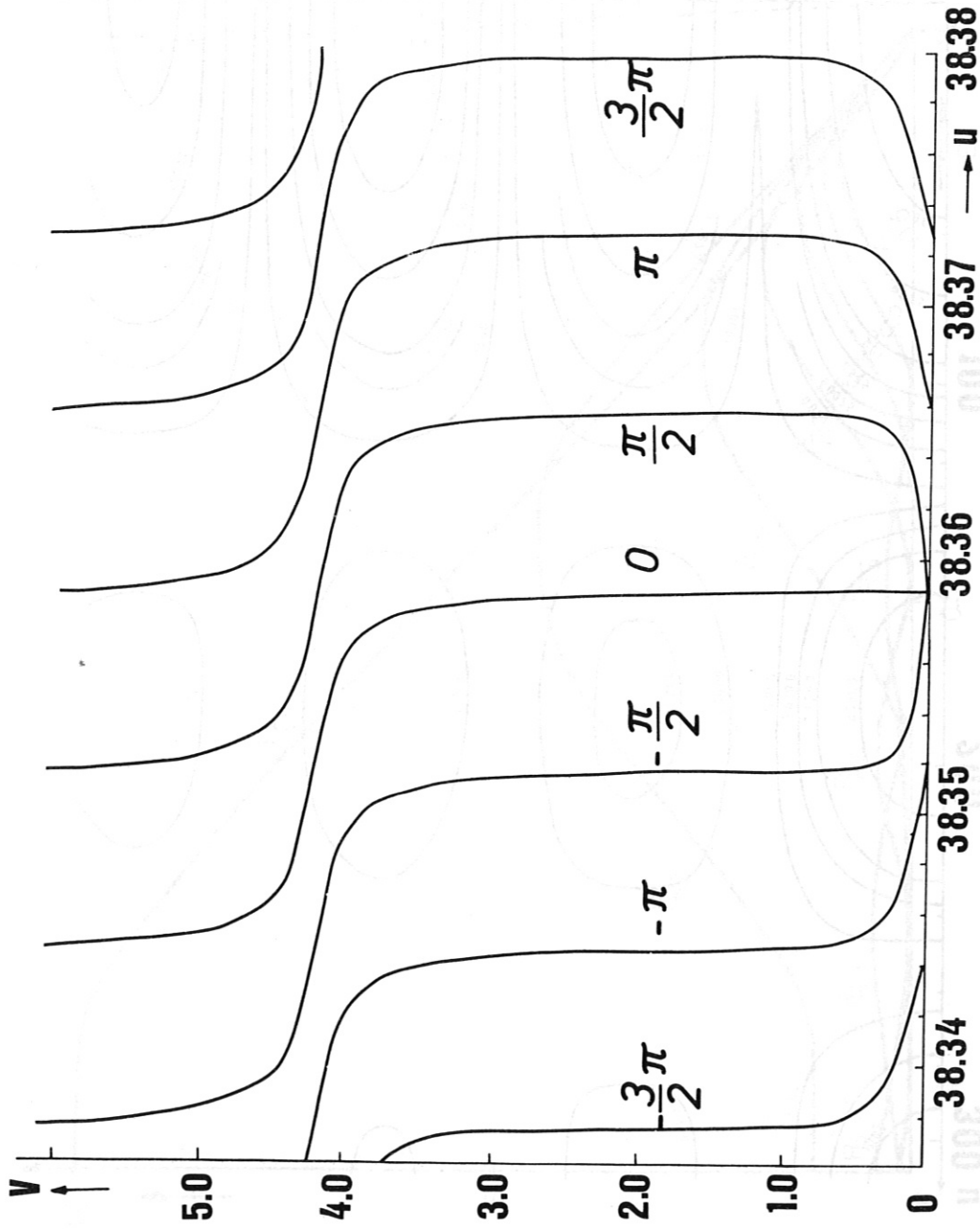

Fig. 10 Co-phasal surfaces around the first axial node (point of zero intensity) for an obstruction coefficient $\varepsilon = 0.817$ and $f/a = 15$.

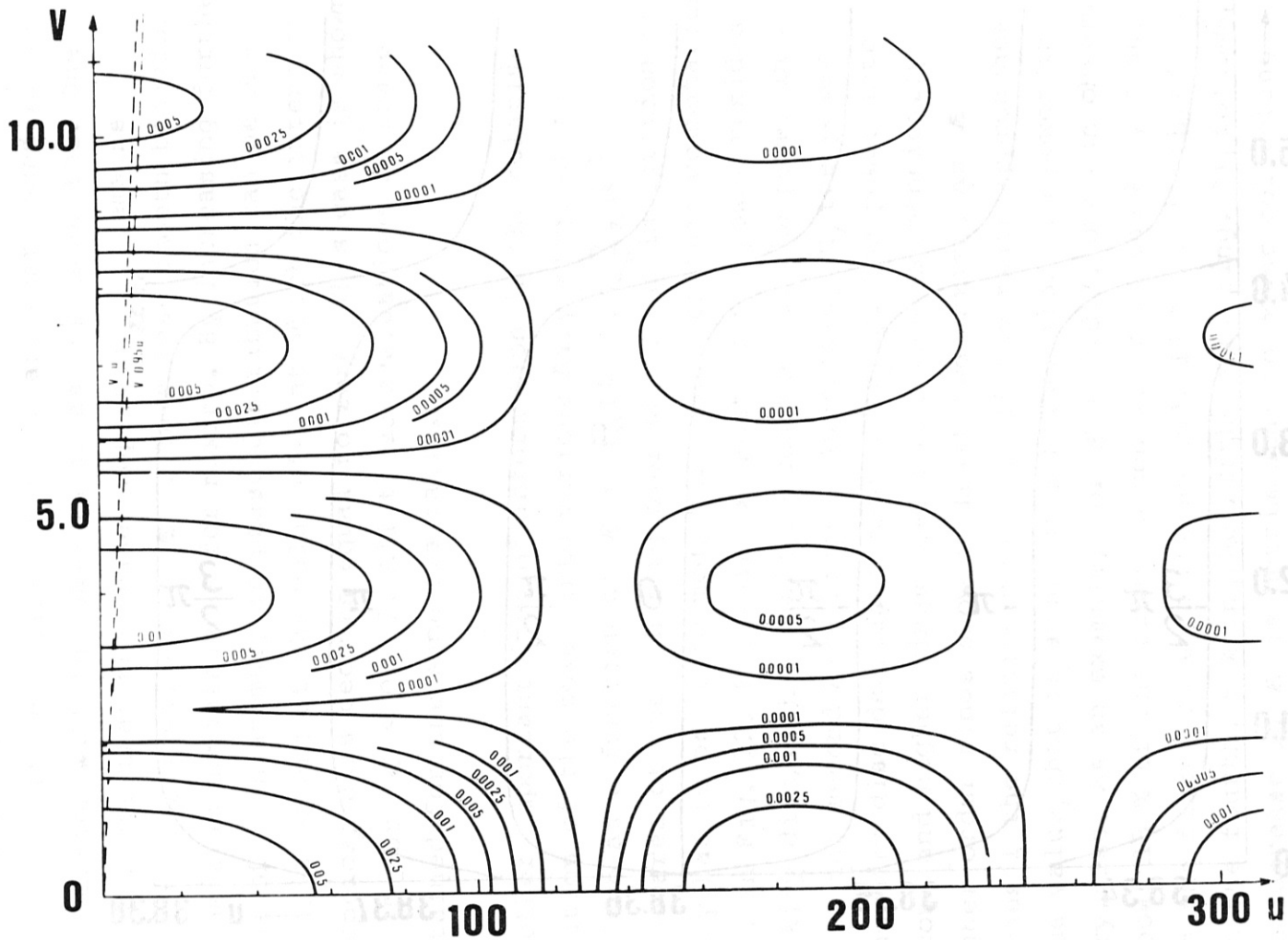

Fig. 11 Isophotes near the focus of an aberration-free pencil for an obstruction coefficient $\varepsilon = 0.95$.

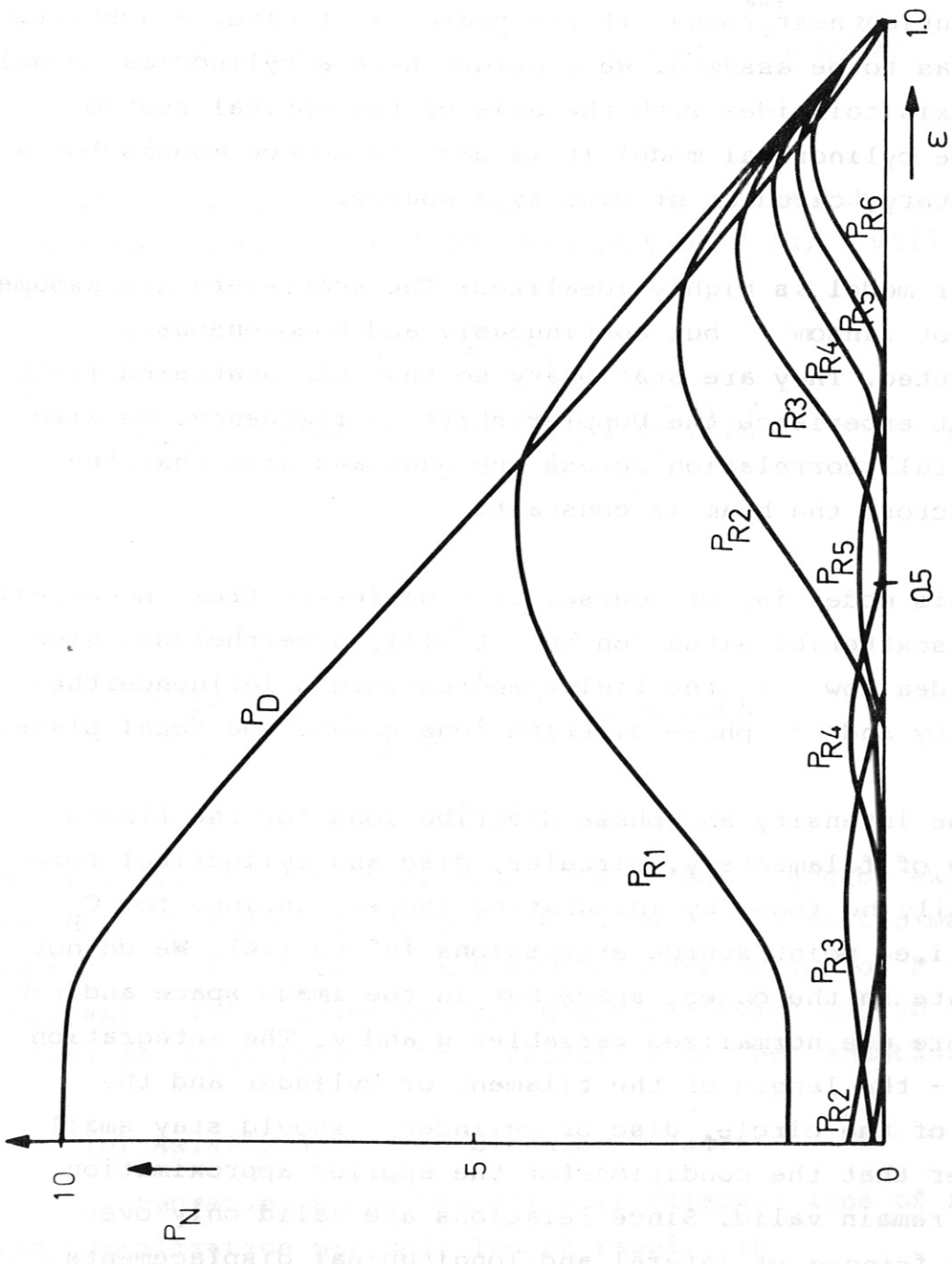

Fig. 12 Integral intensity into various Airy rings as a function of the obstruction coefficient ε.

IV. Finite Size Source

A) Model and Method

To investigate the effect on the intensity and phase distributions near the focus if the source is finite, a scattering model has to be assumed. We consider here a cylindrical model whose axis coincides with the axis of the optical system. From the cylindrical model it is easy to deduce models for a filamentary, circular or disc type source.

Our model is highly idealized: The scatterers are assumed to be not randomly but continuously and homogeneously distributed. They are stationary so that the scattered light does not experience the Doppler shift in frequency. We also assume full correlation across the beam and also that the power across the beam is constant.

This model is, of course, very different from the actual plasma scattering situation but it will, nevertheless, give us an idea how the finite source volume influences the intensity and phase distributions around the focal plane.

The intensity and phase distributions for the finite sources of filamentary, circular, disc and cylindrical form can easily be found by integrating the expressions for C_p and S_p, i.e. point source expressions (9) to (14). We do not integrate in the object space but in the image space and therefore use normalized variables u and v. The integration limits - the length of the filament or cylinder and the radius of the circle, disc or cylinder - should stay small in order that the conditions for the applied approximation method remain valid. Since relations are valid only over several fringes of lateral and longitudinal displacements,

it follows that the size of the source should not violate these conditions. These conditions automatically insure that another condition is satisfied: that the lateral and longitudinal magnification is constant over the object dimensions.

The relations for various sources are now given:

(a) Axial Filament

If the length of the filament is $2u_o$, then the integrated values for C and S at the position P (u,v) will be given by

$$C_F(u,v) = \frac{1}{2u_o} \int_{u-u_o}^{u+u_o} C_p(u',v)\, du' \qquad (22)$$

$$S_F(u,v) = \frac{1}{2u_o} \int_{u-u_o}^{u+u_o} S_p(u',v)\, du' , \qquad (23)$$

where C_p and S_p are point source functions given by expressions (9) to (14) and u' is the distance between the infinitesimal element du' on the filament image and the projection of P (u,v) on the u-axis. The expressions are normalized with $2u_o$ to obtain values per unit length. The variable v is kept constant.

(b) Axially Symmetric Circular Filament

Integration along the circular filament line of radius v_o and normalization per unit length result in

$$C_k(u,v) = \frac{1}{\pi}\int_0^{\pi} d\varphi_o \, C_p(u,v') \tag{24}$$

$$S_k(u,v) = \frac{1}{\pi}\int_0^{\pi} d\varphi_o \, S_p(u,v'), \tag{25}$$

where

$$v' = \sqrt{v^2 + v_o^2 - 2vv_o\cos\varphi_o}$$

is the distance between the "source" element $v_o d\varphi_o$ on the circular filament image $v = v_o$ and the observation point P (u,v), and φ_o is the angular coordinate of this element. The integration is performed in the u = const plane.

(c) Axially Symmetric Thin Disc Source

Consider a disc source image of radius v_o. The integration is performed as indicated in Fig. 13. Depending on whether the size of the disc image v_o is smaller or larger than the radial distance v of the observation point P (u,v) from the axis, we will have two different expressions for C_D and S_D.

1. $v \geq v_o$

Point P (u,v) is outside the image disc. Then

$$C_D(u,v) = \frac{2}{\pi v_o^2}\int_{v-v_o}^{v+v_o} C_p(u,v') \arccos\left[\frac{v^2 + v'^2 - v_o^2}{2vv'}\right] v' dv' \tag{26}$$

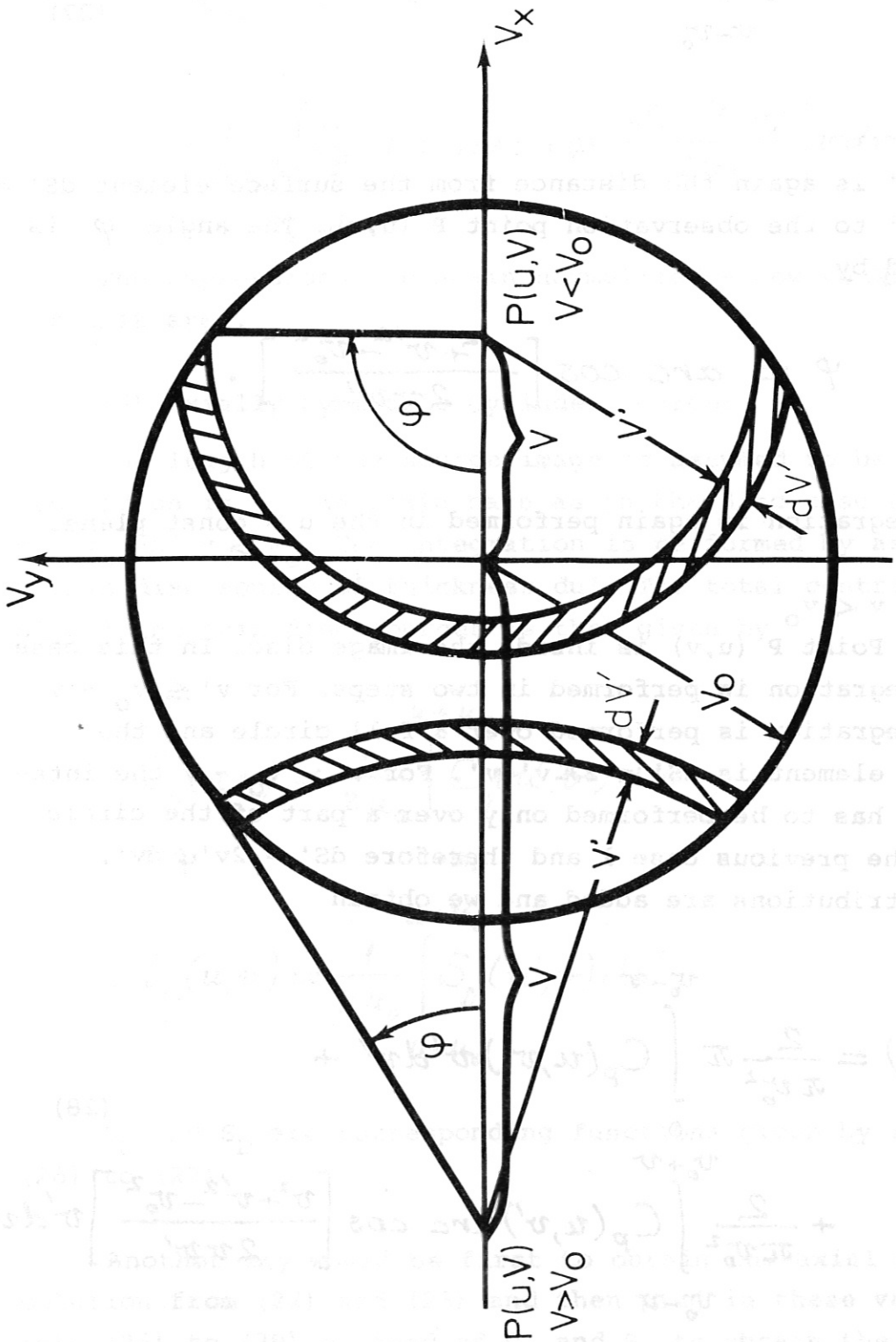

Fig. 13 Sketch of integration method for a thin disc source.

$$S_D(u,v) = \frac{2}{\pi v_0^2} \int_{v-v_0}^{v+v_0} S_p(u,v) \arccos\left[\frac{v^2+v'^2-v_0^2}{2vv'}\right] v' dv', \tag{27}$$

where v' is again the distance from the surface element dS' = 2v'φ dv' to the observation point P (u,v). The angle φ is replaced by

$$\varphi = \arccos\left[\frac{v^2+v'^2-v_0^2}{2vv'}\right].$$

The integration is again performed in the u = const plane.

2. $v < v_0$

Point P (u,v) is inside the image disc. In this case the integration is performed in two steps. For $v' \leq v_0 - v$ the integration is performed over a full circle and the surface element is dS' = $2\pi v' dv'$. For $v' > v_0 - v$ the integration has to be performed only over a part of the circle as in the previous case 1 and therefore dS' = 2v'φ dv'. Two contributions are added and we obtain

$$C_D(u,v) = \frac{2}{\pi v_0^2} \pi \int_0^{v_0-v} C_p(u,v') v' dv' + \tag{28}$$

$$+ \frac{2}{\pi v_0^2} \int_{v_0-v}^{v_0+v} C_p(u,v') \arccos\left[\frac{v^2+v'^2-v_0^2}{2vv'}\right] v' dv'$$

$$S_D(u,v) = \frac{2}{\pi v_o^2}\pi \int_0^{v_o - v} S_p(u,v')\,v'dv' +$$

$$+ \frac{2}{\pi v_o^2} \int_{v_o - v}^{v_o + v} S_p(u,v') \arccos\left[\frac{v^2 + v'^2 - v_o^2}{2vv'}\right] v'dv'. \quad (29)$$

The expressions are again normalized - now to πv_o^2, i.e. per unit area.

(d) Axially Symmetric Cylinder Source:

The length of the source image is assumed to be $2u_o$ and its radius is v_o. We again have as in the disc case two regions: $v \geq v_o$ and $v \leq v_o$. The integration is performed by assuming a thin disc source of thickness du'. The total contribution of all the thin disc sources is then given by

$$C_c(u,v) = \frac{1}{2u_o} \int_{u-u_o}^{u+u_o} C_D(u',v)\,du' \quad (30)$$

$$S_c(u,v) = \frac{1}{2u_o} \int_{u-u_o}^{u+u_o} S_D(u',v)\,du'. \quad (31)$$

C_D and S_D are corresponding functions given by relations (26) to (29).

Another way would be first to obtain the axial filament solution from (22) and (23) and then plug in these values into (26) to (29) instead of C_p and S_p to obtain the cylinder source distributions. This is actually the method that was

used to obtain the numerical results.

The intensity and phase distributions for each one of these cases is obtained simply by inserting the corresponding C's and S's into expressions (15) and (16).

B) Results of Computation

All four kinds of sources were numerically investigated but results will be presented only for the cylindrical case. The obstruction coefficient ε, the source image length $2u_o$ and radius v_o were varied to study their influence on the intensity and phase distributions. The F-number of the lens was kept constant, f/a = 15. Three groups of results are described in which ε was kept constant - ε = 0.01, 0.4 and 0.817 - and u_o and v_o were varied.

If the size of the source is increased radially and/or axially, one should expect a flattening of the intensity distribution and an increase in the size of the Airy disc to occur. The Airy disc becomes the image of the source and should have the size of the source image. The co-phasal surfaces across the image should straighten out. This, on the other hand, would mean that the size of the mixer can be increased to the size of the image, thereby increasing the collected power and the signal without impairing the mixing efficiency, which depends on the phase distributions of the scattered and local oscillator waves across the mixer.

If the aperture blocking is kept very small, this is exactly what is observed. The computational results for ε = 0.01 are shown in Figs. 14 to 21 . Comparing isophote figures 14 to 17 with the point source case of the same ε in Fig. 5 , one can observe flattening of the isophotes and increased loss of detail. As either u_o or v_o or both are increased a plateau in the focal plane slowly appears enlarging the Airy disc.Keeping v_o = 3 constant and increasing the length of the cylinder from $2u_o$ = 3 to 18, the size of the Airy disc - as shown in Figs. 14 to 16 - increases from v_D = 4.8 to 6.4. An interesting result happens if v_o is kept equal to 6 and $2u_o$ is increased again from 0 to 18.Two examples are shown in Figs. 17 and 18 . Instead of an intensity maximum on the optical axis at u = 0 (focal point) the maximum shifts suddenly to u = 9. Increasing $2u_o$, this maximum slowly disappears and at $2u_o$ = 18 the maximum appears again at the focal point. At the same time the size of the Airy disc increases from about 8 to about 10.

Keeping the length of the cylinder constant - $2u_o$ = 6 - and increasing the radius from v_o = 1 to 6 will change the isophote structure very strongly: They are smoothed out, with many local maxima and minima disappearing and the focal plane plateau becoming distinct. The Airy disc radius v_D increases very drastically: from about 4 to about 8.2.

The change in co-phasal lines for ε = 0.01 and for the variables v_o and u_o is shown in Figs. 19 to 21 . In each figure either v_o or u_o is kept constant and the other is changed parametrically. For the extreme values of the parameter - maximum and minimum - two co-phasal lines are shown separated by a phase difference of π . The other values of the parameter are represented only by one co-phasal line. For v_o = 3 and $2u_o$ changed from 3 to 18 - see Fig. 19 - the co-phasal lines straighten out monotonically with increased u_o.

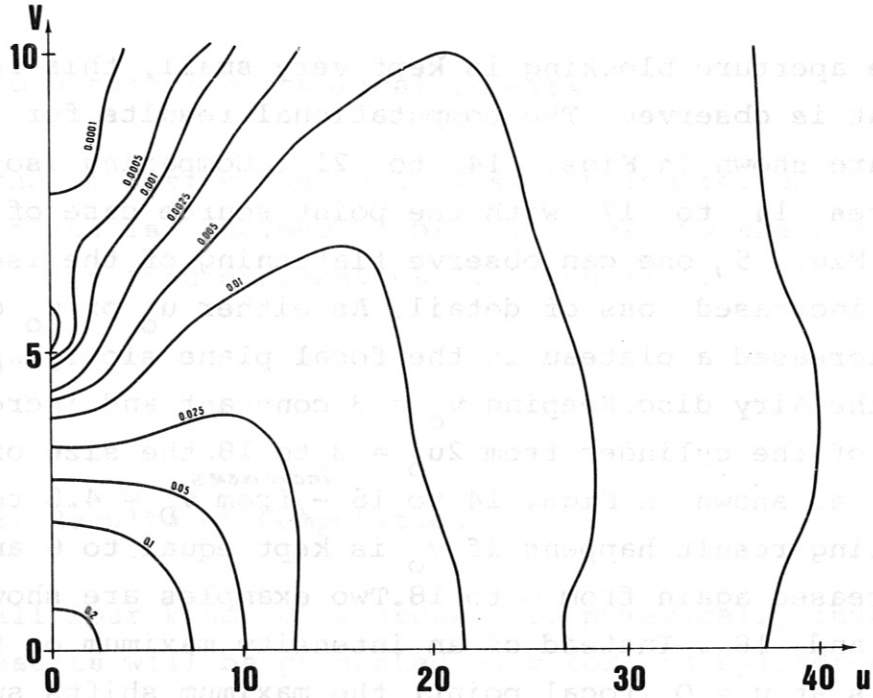

Fig. 14 Isophotes near the focus for an obstruction coefficient ε = 0.01. The source is a cylinder of length $2u_o$ = 3 and of radius v_o = 3.

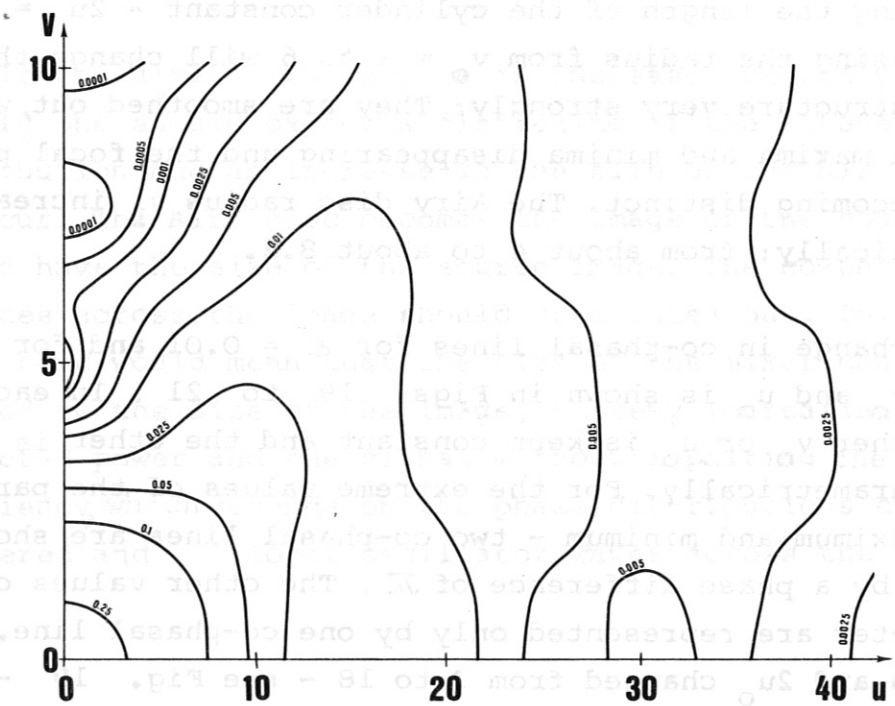

Fig. 15 Isophotes near the focus for an obstruction coefficient ε = 0.01. The source is a cylinder of length $2u_o$ = 9 and of radius v_o = 3.

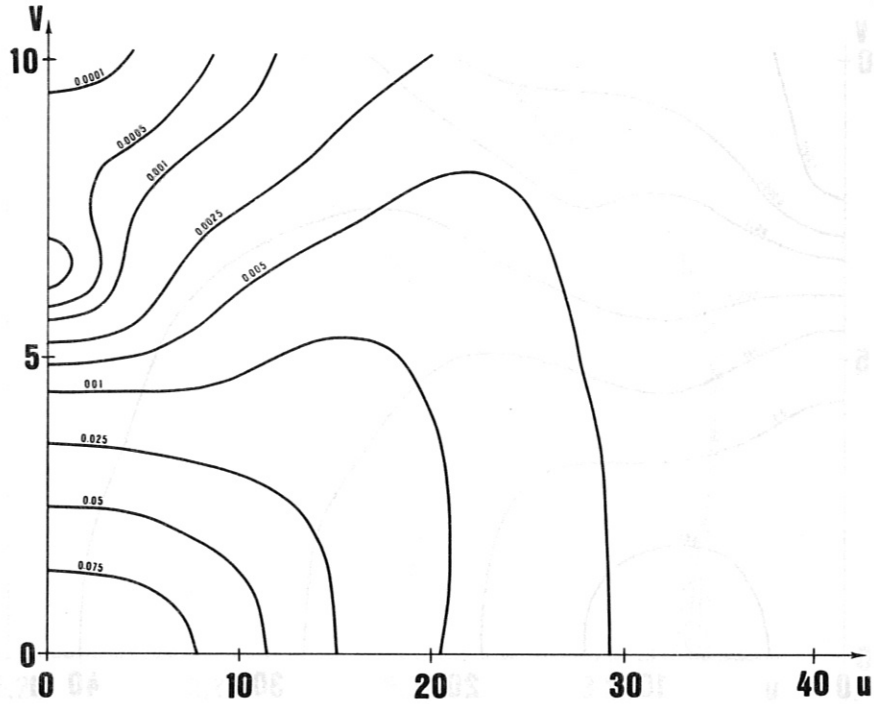

Fig. 16 Isophotes near the focus for an obstruction coefficient ε = 0.01. The source is a cylinder of length $2u_o$ = 18 and of radius v_o = 3.

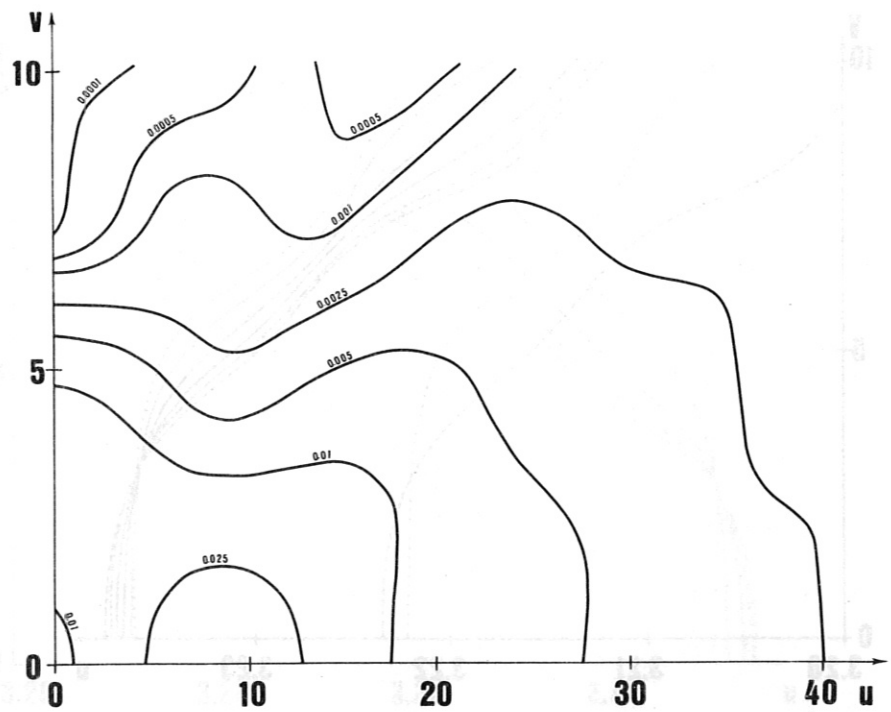

Fig. 17 Isophotes near the focus for an obstruction coefficient ε = 0.01. The source is a disc of radius v_o = 6.

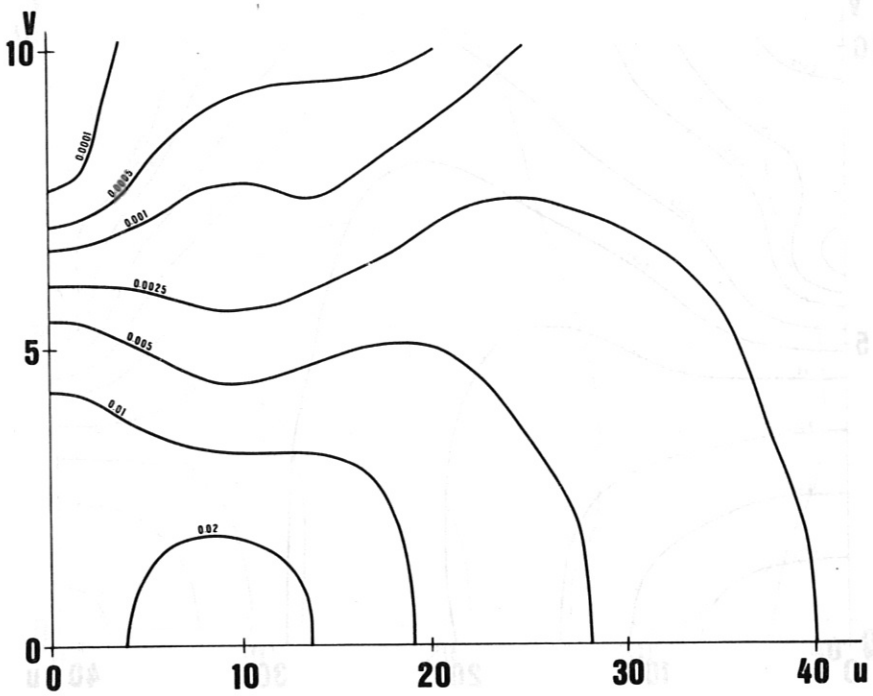

Fig. 18 Isophotes near the focus for an obstruction coefficient ε = 0.01. The source is a cylinder of length $2u_o$ = 9 and of radius v_o = 6.

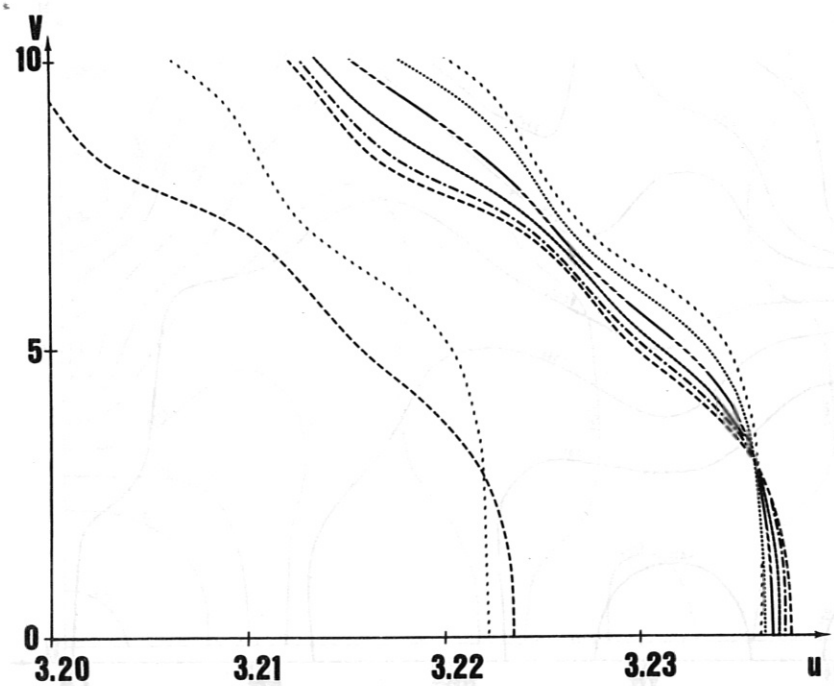

Fig. 19 Co-phasal surfaces in the neighborhood of u = 3.2 for an obstruction coefficient ε = 0.01 and f/a = 15. The source is a cylinder of radius v_o = 3. The length of the source varies: 1 - $2u_o$ = 3, 2 - $2u_o$ = 6, 3 - $2u_o$ = 9, 4 - $2u_o$ = 12, 5 - $2u_o$ = 15 and 6 - $2u_o$ = 18. The distance between the two sets of curves is π.

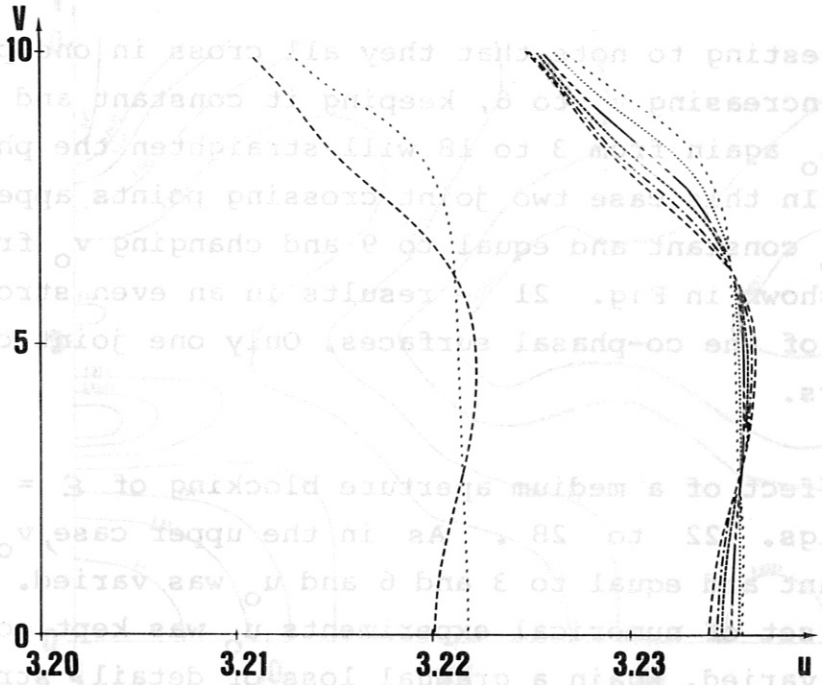

Fig. 20 Co-phasal surfaces in the neighborhood of u = 3.2 for an obstruction coefficient ε = 0.01 and f/a = 15. The source is a cylinder of length $2u_o$ = 9. The radius v_o of the source is varied and its values are indicated in the figure.

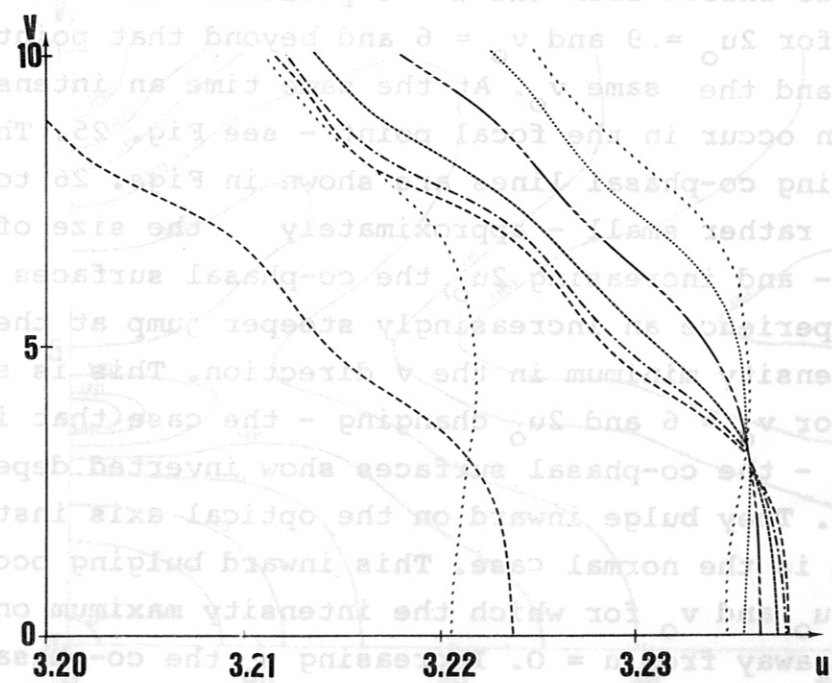

Fig. 34 Co-phasal surfaces in the neighborhood of u = 9.1 for an obstruction coefficient ε = 0.817 and f/a = 15. The source is a cylinder of length $2u_o$ = 9. The radius v_o of the source is varied and its values are indicated in the figure.

It is interesting to note that they all cross in one point at $v \approx 3$. Increasing v_o to 6, keeping it constant and changing $2u_o$ again from 3 to 18 will straighten the phase even more. In this case two joint crossing points appear. Keeping $2u_o$ constant and equal to 9 and changing v_o from 1 to 6 - as shown in Fig. 21 - results in an even stronger flattening of the co-phasal surfaces. Only one joint crossing point occurs.

The effect of a medium aperture blocking of $\varepsilon = 0.4$ is shown in Figs. 22 to 28 . As in the upper case, v_o was kept constant and equal to 3 and 6 and u_o was varied. Also in another set of numerical experiments u_o was kept constant and v_o was varied. Again a gradual loss of detail, straightening of the isophotes and co-phasal lines can be observed. This is especially evident in the u-direction. A rather surprising result is that the change in the radial direction is small. By increasing v_o or u_o the Airy disc does not grow correspondingly but stays small At certain values of u_o and v_o the maximum in the focus shifts from the $u = 0$ position toward some finite u: to $u = 11$ for $2u_o = 9$ and $v_o = 6$ and beyond that point for even higher u_o and the same v_o. At the same time an intensity minimum can occur in the focal point - see Fig. 25. The corresponding co-phasal lines are shown in Figs. 26 to 28. Keeping v_o rather small - approximately the size of the Airy disc - and increasing $2u_o$, the co-phasal surfaces straighten out but experience an increasingly steeper jump at the position of the intensity minimum in the v direction. This is shown in Fig. 26. For $v_o = 6$ and $2u_o$ changing - the case that is shown in Fig. 27 - the co-phasal surfaces show inverted dependence on u and v. They bulge inward on the optical axis instead of forward as is the normal case. This inward bulging occurs at values of u_o and v_o for which the intensity maximum on the axis moves away from $u = 0$. Increasing u_o, the co-phasal surfaces again become more straight but experience a sudden steeper

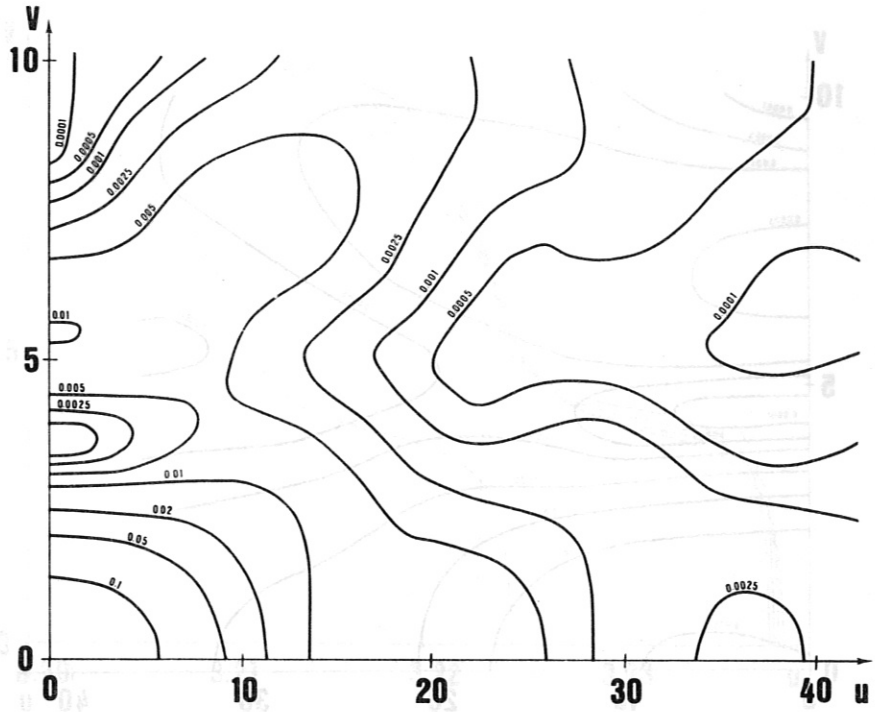

Fig. 22 Isophotes near the focus for an obstruction coefficient ε = 0.4. The source is a cylinder of length $2u_o$ = 3 and of radius v_o = 3.

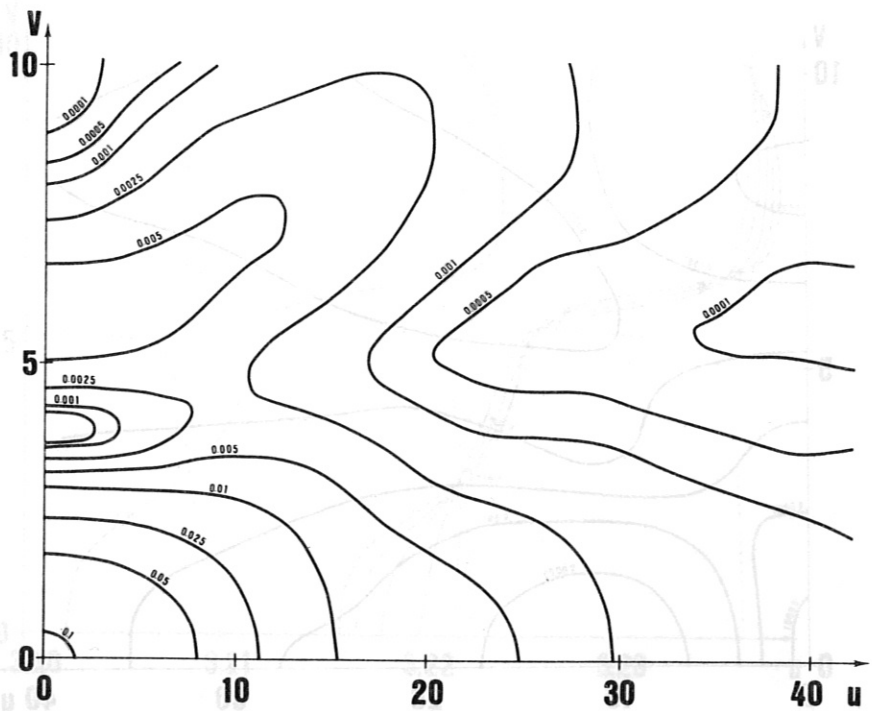

Fig. 23 Isophotes near the focus for an obstruction coefficient ε = 0.4. The source is a cylinder of length $2u_o$ = 9 and of radius v_o = 3.

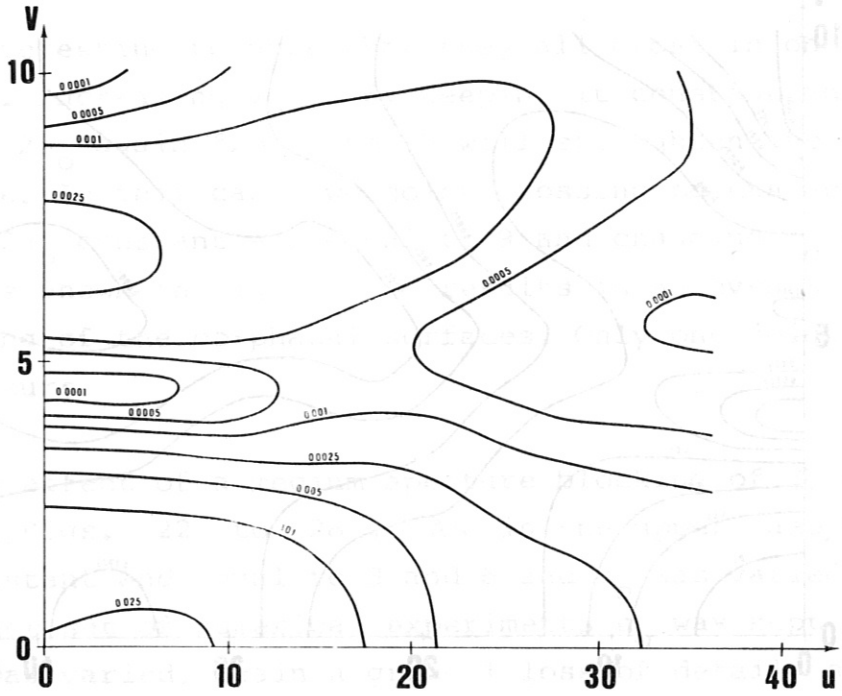

Fig. 24 Isophotes near the focus for an obstruction coefficient ε = 0.4. The source is a cylinder of length $2u_o$ = 18 and of radius v_o = 3.

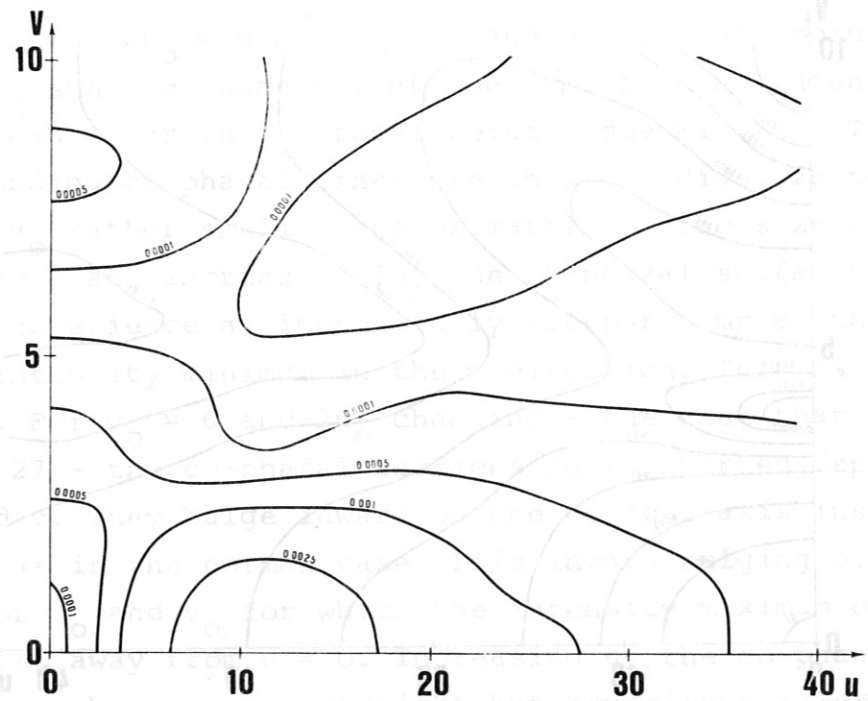

Fig. 25 Isophotes near the focus for an obstruction coefficient ε = 0.4. The source is a cylinder of length $2u_o$ = 9 and of radius v_o = 6.

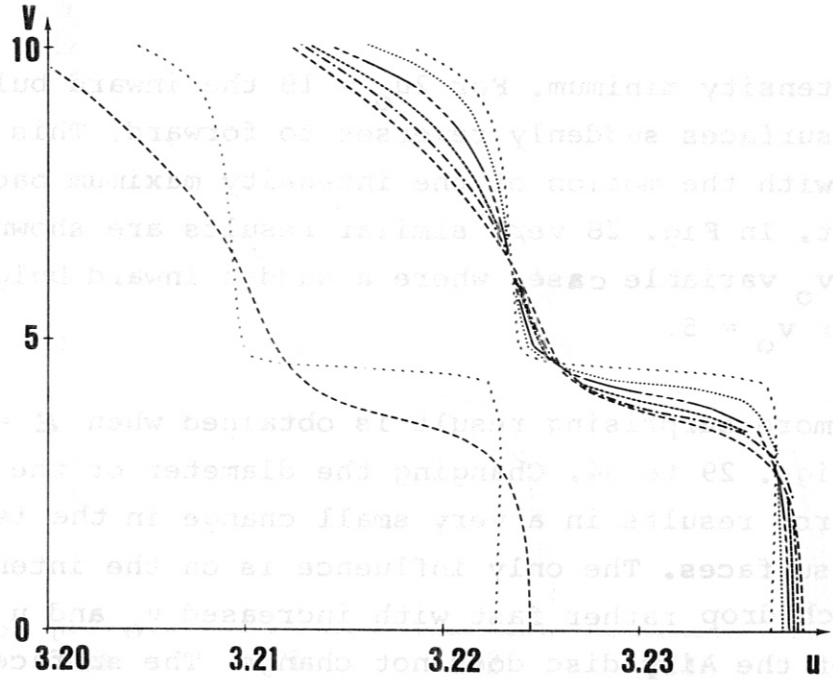

Fig. 26 Co-phasal surfaces in the neighborhood of u = 3.2 for an obstruction coefficient $\mathcal{E}$ = 0.4 and f/a = 15. The source is a cylinder of radius v_o = 3. The length of the source varies: 1 - $2u_o$ = 3, 2 - $2u_o$ = 6, 3 - $2u_o$ = 9, 4 - $2u_o$ = 12, 5 - $2u_o$=15 and 6 - $2u_o$ = 18. The distance between the two sets of curves is π.

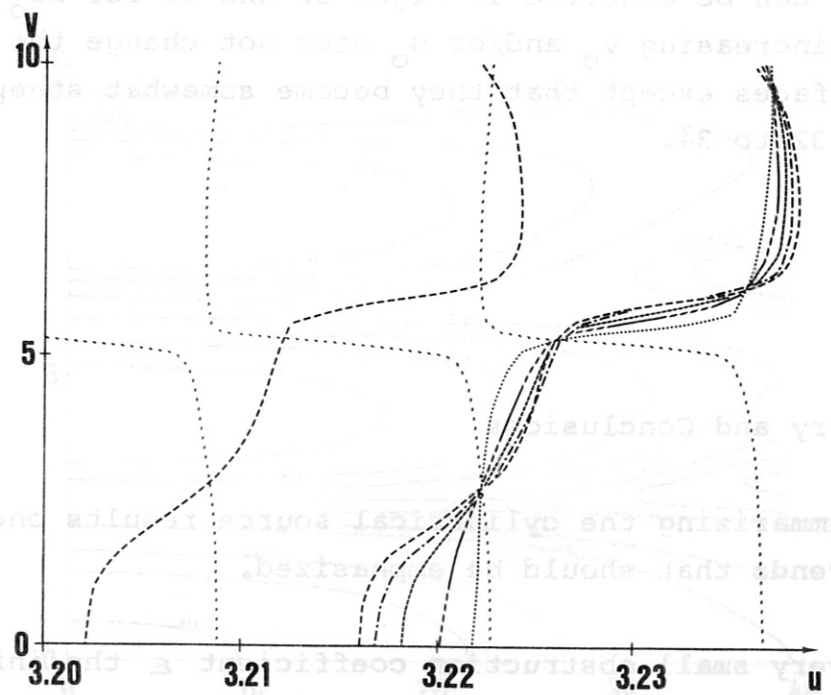

Fig. 27 Co-phasal surfaces in the neighborhood of u = 3.2 for an obstruction coefficient $\mathcal{E}$ = 0.4 and f/a = 15. The source is a cylinder of radius v_o = 6. The length of the source varies: 1 - $2u_o$ = 3, 2 - $2u_o$ = 6, 3 - $2u_o$ = 9, 4 - $2u_o$ = 12, 5 - $2u_o$=15 and 6 - $2u_o$ = 18.

jump in the intensity minimum. For $2u_o = 18$ the inward bulge in the co-phasal surfaces suddenly reverses to forward. This coincides with the motion of the intensity maximum back to the $u = 0$ point. In Fig. 28 very similar results are shown for $u_o = 4.5$, v_o variable case, where a sudden inward bulge appears for $v_o = 5$.

An even more surprising result is obtained when $\varepsilon = 0.817$, shown in Figs. 29 to 34. Changing the diameter or the length of the source results in a very small change in the isophotes or co-phasal surfaces. The only influence is on the intensity values, which drop rather fast with increased v_o and u_o. The position of the Airy disc does not change. The surfaces are not flattened out and the amount of detail in the isophote distribution stays the same. The only change occurs when $2u_o$ is increased to about 15 (see Fig. 30). Here the intensity maximum shifts from the focal point to $u \approx 25$. This is accompanied by sudden inward bulging of the co-phasal surfaces, as can be observed in Figs. 32 and 33 for $2u_o = 15$. Otherwise increasing v_o and/or u_o does not change the co-phasal surfaces except that they become somewhat steeper - see Figs. 32 to 34.

V. Summary and Conclusions

In summarizing the cylindrical source results one notes several trends that should be emphasized.

For very small obstruction coefficient ε the influence of increasing the size of the source is very strong: The isophote diagrams become smoother, a central plateau builds up

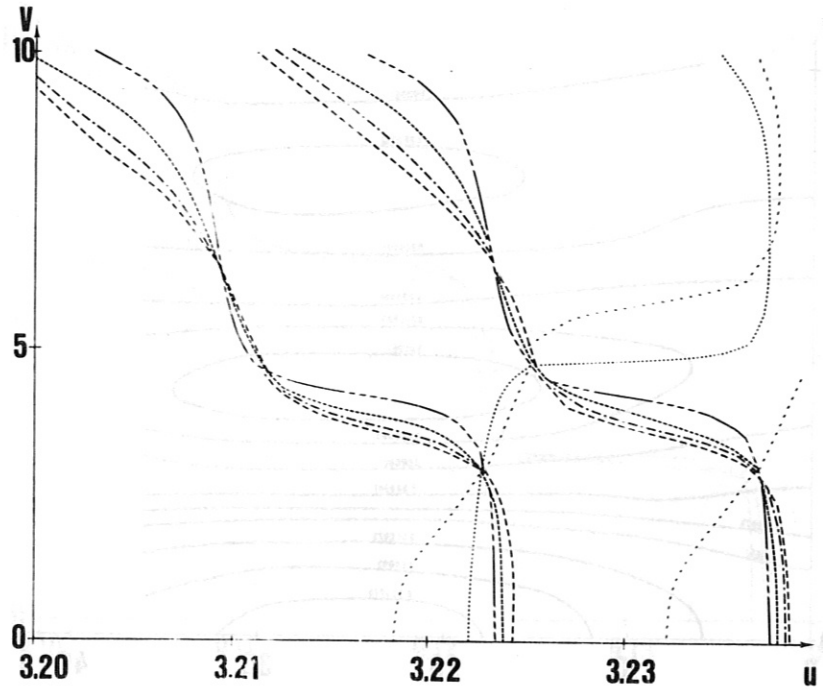

Fig. 28 Co-phasal surfaces in the neighborhood of u = 3.2 for an obstruction coefficient ε = 0.4 and f/a = 15. The source is a cylinder of length $2u_o$ = 9. The radius v_o of the source is varied and its values are indicated in the figure.

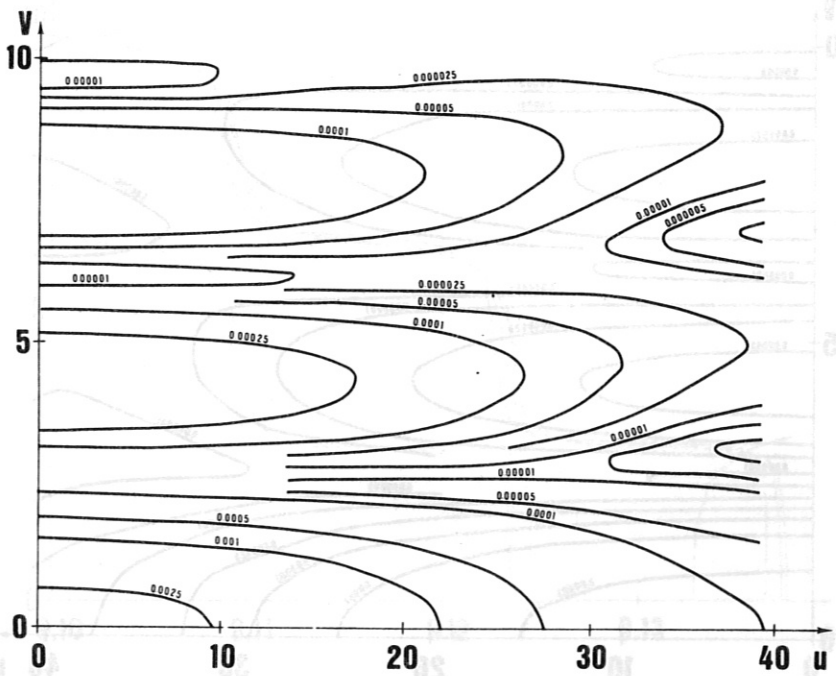

Fig. 29 Isophotes near the focus for an obstruction coefficient ε = 0.817. The source is a cylinder of length $2u_o$ = 9 and of radius v_o = 3.

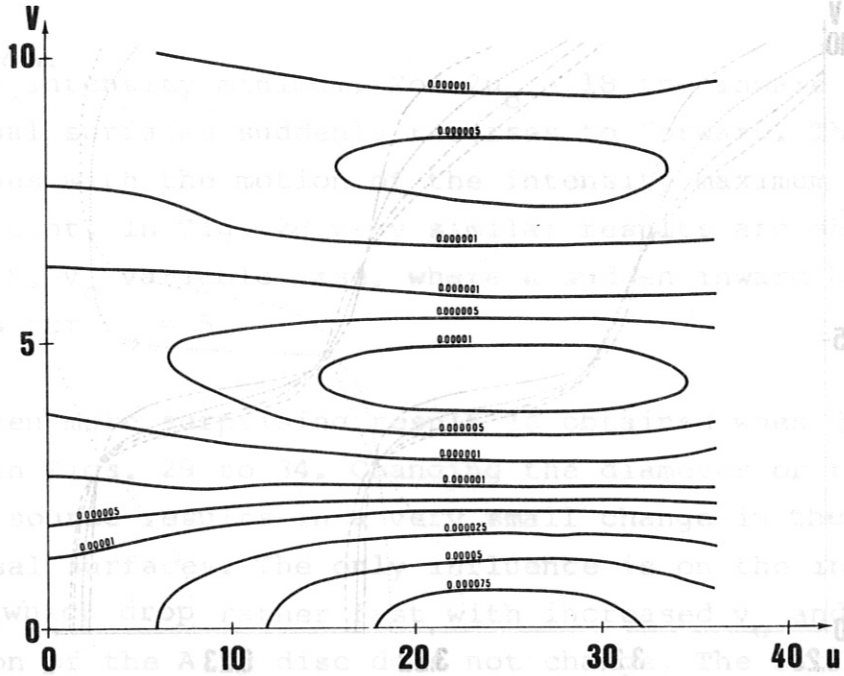

Fig. 30 Isophotes near the focus for an obstruction coefficient ε = 0.817. The source is a cylinder of length $2u_o$ = 15 and of radius v_o = 3.

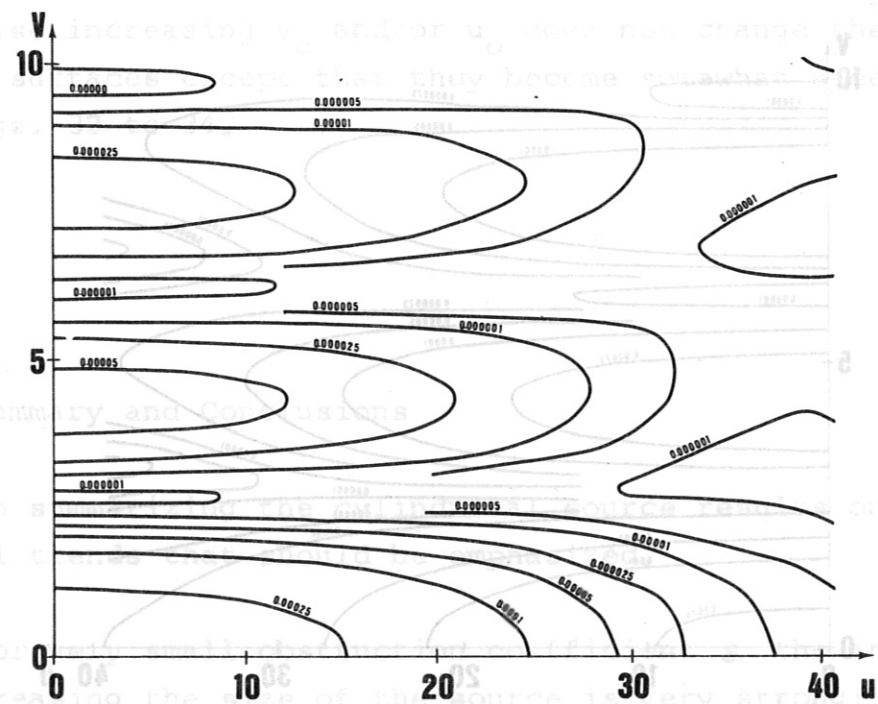

Fig. 31 Isophotes near the focus for an obstruction coefficient ε = 0.817. The source is a cylinder of length $2u_o$ = 9 and of radius v_o = 6.

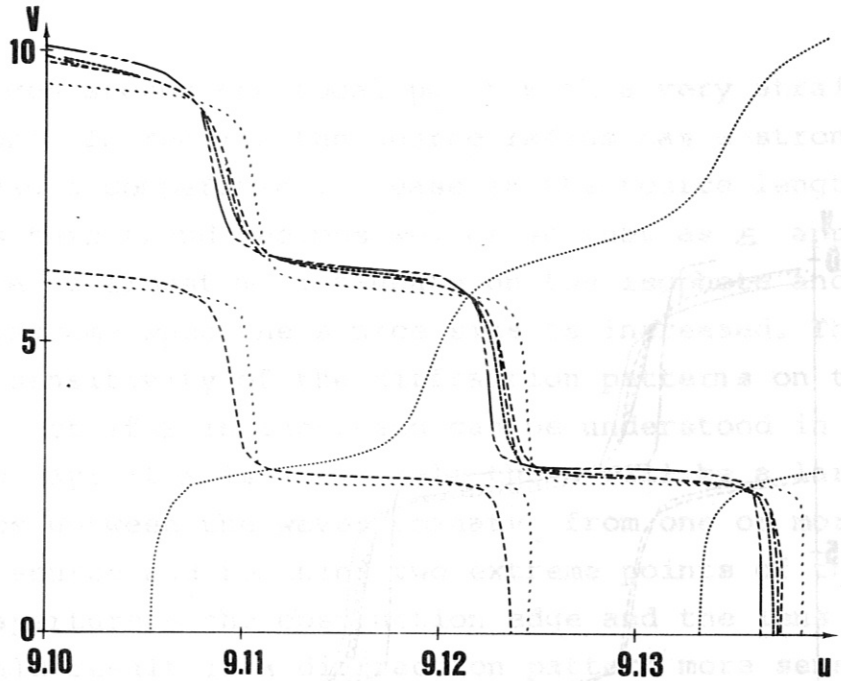

Fig. 32 Co-phasal surfaces in the neighborhood of u = 9.1 for an obstruction coefficient $\mathcal{E}$ = 0.817 and f/a = 15. The source is a cylinder of radius v_o = 3. The length of the source varies: 1 - $2u_o$ = 3, 2 - $2u_o$ = 6, 3 - $2u_o$ = 9, 4 - $2u_o$ = 12, 5 - $2u_o$ = 15, and 6 - $2u_o$ = 18. The distance between the two sets of curves is π .

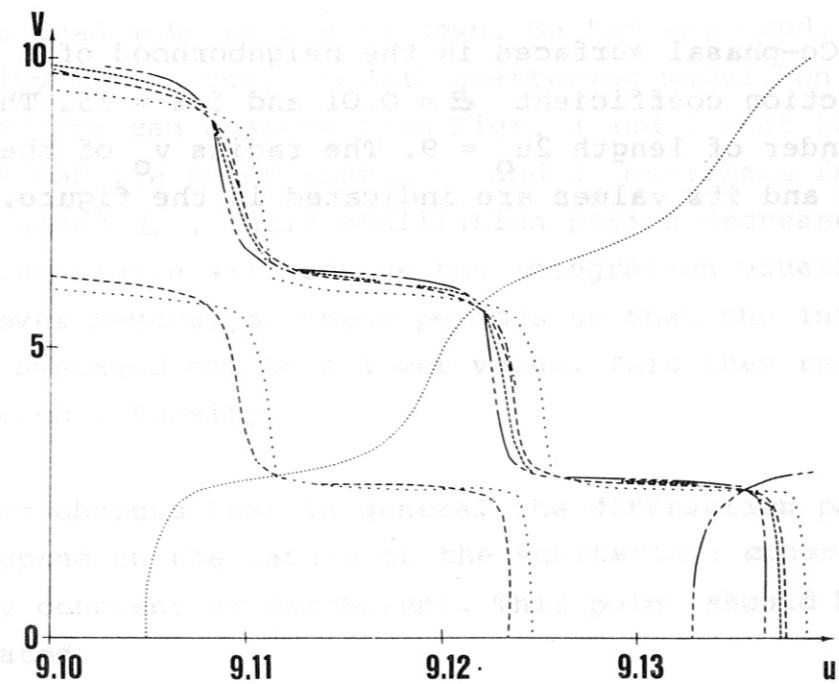

Fig. 33 Co-phasal surfaces in the neighborhood of u = 9.1 for an obstruction coefficient $\mathcal{E}$ = 0.817 and f/a = 15. The source is a cylinder of radius v_o = 6. The length of the source varies: 1 - $2u_o$ = 3, 2 - $2u_o$ = 6, 3 - $2u_o$ = 9, 4 - $2u_o$ = 12, 5 - $2u_o$ = 15, and 6 - $2u_o$ = 18.

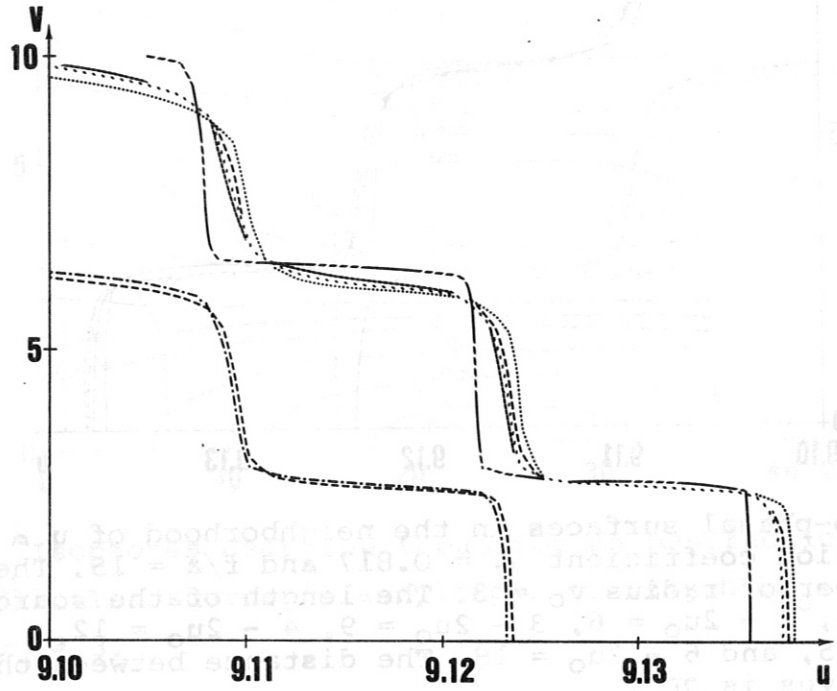

Fig. 21 Co-phasal surfaces in the neighborhood of u = 3.2 for an obstruction coefficient $\mathfrak{E}$ = 0.01 and f/a = 15. The source is a cylinder of length $2u_o$ = 9. The radius v_o of the source is varied and its values are indicated in the figure.

and enlarges around the focal point with a very straight phase front. Increasing the source radius has a stronger effect than a comparable increase in the source length. As ε increases this trend becomes weaker so that as ε approaches there is almost no influence on the isophote and cophasal diagrams when the source size is increased. This diminished sensitivity of the diffraction patterns on the size of the object if ε is increased can be understood in the following way: if ε is very small, there will be a large phase difference between the waves emanating from one or more points of the source and reaching two extreme points of the annular aperture - the obstruction edge and the lens edge. This should result in a diffraction pattern more sensitive to the values of the source length and radius. As ε approaches 1 this phase difference becomes smaller with the result that the diffraction pattern is less sensitive to the size of the source.

It is also observed that as the source size is increased the normalized intensities go down. On the one hand, this is a peculiarity of our very special scattering model. On the other hand, one can observe from Figs. 3 and 4 that the functions for the point source C_p and S_p oscillate faster with increased ε. Their oscillation period decreases. In the case of the finite size source the integration usually extends over several of these periods so that the integrated value is averaged out to a lower value. This then results in a lowered intensity.

It is obvious that in general the diffraction pattern should depend on the nature of the scattering: coherent, partially coherent or incoherent. This point should be further investigated.

For very small ε the angular alignment of the signal beam (scattered radiation) and the local oscillation beam has, as usual, to be rather accurate. On the other hand, the radial alignment of these two beams is not so crucial. The size of the mixer should be equal to the enlarged Airy disc diameter. This would guarantee that the phase difference between the signal and the local oscillator waves across the mixer is constant. The local oscillator could be either a plane wave or a wave focused on the mixer with an appropriate phase distribution.

If the aperture blocking is large - as is the case in extreme forward scattering - the size of the central plateau (Airy disc) is very small and it carries only a fraction of the signal beam power. It is now more difficult to achieve radial alignment. Mixing can now be achieved in two ways:

1. The size of the mixer is equal to the size of the Airy disc. For the Gondhalekar-Keilmann proposal this would mean a mixer with a diameter of 0.07 mm. The signal power incident on the mixer is only about 17 % of the input power; the rest is lost on other diffraction rings. The advantage of this method is that the local oscillator can be either a plane wave or a focused wave.

2. The size of the mixer is increased to cover 5 to 7 diffraction rings. Now most of the signal power is utilized. The signal and local oscillator beams have to be very accurately aligned - the allowed error being only a fraction of the Airy disc. This means that for the Gondhalekar-Keilmann proposal the allowed error would be about 10 μm. The signal and local oscillator waves have to be focused with a lens of the same f/a number and, furthermore, the local oscillator optics has to have the same obstruction coefficient as the signal optics. The alignment in angle between the signal and the local oscillator has to have the usual accuracy.

References

1. A. Gondhalekar and F. Keilmann, Report Nr. IPP 2/201, IPP IV/26, Max-Planck-Institut für Plasmaphysik, Garching, August 1971.

2. E. v. Lommel, Abh. der Bayerischen Akad., 53, p. 233 (1885).

3. H. Struve, Mém. de l'Acad.de St. Petersbourg (7), 34, No. 5, 1 (1886).

4. E. Zernike and B.R.A. Nijboer, Contribution to "Théorie des images optique", p. 227, Éditions de la Revue d'Optique, Paris (1949).

5. E. H. Linfoot and E. Wolf, Mon.Not.Roy.Astr.Soc., 112, p. 452 (1952).

6. E. H. Linfoot and E. Wolf, Proc.Phys.Soc., Section B, 66, p. 145 (1953).

7. G. C. Steward, Phil.Trans.Roy.Soc. A, 225, p. 131 (1925).

8. E. H. Linfoot and E. Wolf, Proc.Phys.Soc., Section B, 69, p. 823 (1956).